Relaxing Limits from Big Bang Nucleosynthesis on Heavy Neutral Leptons with Axion-like Particles

Frank F. Deppisch,[a] **Tomás E. Gonzalo,**[b] **Chayan Majumdar,**[a] **Zhong Zhang**[a]

[a]*Department of Physics and Astronomy, University College London,*
London WC1E 6BT, United Kingdom

[b]*Institute for Theoretical Particle Physics (TTP), Karlsruhe Institute of Technology (KIT), 76128*
Karlsruhe, Germany

E-mail: f.deppisch@ucl.ac.uk, tomas.gonzalo@kit.edu,
c.majumdar@ucl.ac.uk, zhong.zhang.19@ucl.ac.uk

ABSTRACT: Heavy neutral leptons (HNLs) are constrained by requirements of Big Bang Nucleosynthesis (BBN) as their decays significantly impact the formation of the primordial elements. We propose here a model where the primary decay channel for the HNLs is to an axion-like particle (ALP) and a neutrino. Consequently, HNLs can decay earlier and evade the BBN bound for lower masses, provided the ALPs themselves decay considerably later. Further cosmological and astrophysical constraints limit severely the range of validity of the ALP properties. We find that a new parameter region opens up for HNLs with masses between 1 MeV and 1 GeV, and active-sterile neutrino mixing strengths between 10^{-9} and 10^{-6} that is consistent with constraints and can be probed in future searches. In such a scenario, current bounds as well as sensitivities of future direct HNL searches such as at NA62 and DUNE will be affected.

arXiv:2410.06970v1 [hep-ph] 9 Oct 2024

Contents

1 Introduction

Heavy Neutral Leptons (HNLs) are amongst the most popular exotic particles thought to exist beyond the particle content of the Standard Model (SM). Assumed to be fermions that are neutral under the SM gauge symmetries, they act as heavy right-handed neutrinos and, if they are of Majorana nature, trigger a seesaw mechanism of light neutrino mass generation [1–5]. In this context, they may also help to understand the matter-antimatter asymmetry of the universe, as their CP-violating decays or oscillations can generate a baryon asymmetry through leptogenesis [6]. HNLs may thus help to explain why the active neutrinos are so much lighter than the other SM fermions, but not massless as required from observing oscillations [7, 8], and the origin of matter in the universe.

In the minimal scenario, an HNL N couples to the SM only through its mixing $U_{\alpha N}$ ($\alpha = e, \mu, \tau$) with the active neutrinos, induced by the Yukawa coupling of the HNL with

the SM lepton doublets L_α and Higgs doublet H. The HNL then also participates in charged and neutral lepton currents. There are numerous past, current and planned future searches for HNLs based on this, over a wide range of HNL masses m_N; from the eV-scale where HNLs can be tested in oscillations, over keV and MeV scales mainly probed in nuclear processes such as β decay, MeV to GeV in beam dump and meson decays, to electroweak scale masses and above probed in colliders. A recent overview of current and future searches is provided in [9, 10] and a global study of current constraints on HNLs can be found in [11]. The mass range 100 MeV $\lesssim m_N \lesssim$ 100 GeV has especially been targeted in searches for HNLs, since in this mass range HNLs are naturally long-lived for the small active-sterile mixing strengths expected for successful neutrino mass generation. This results in macroscopic decay lengths and thus displaced decay vertices that can be looked for with a high sensitivity.

Being long-lived, HNLs also affect the early history of the universe beyond their role in leptogenesis. If HNLs had been in thermal equilibrium, and they decay around or later than about a second after the big bang, the produced particles affect Big Bang Nucleosynthesis (BBN) [12, 13]. In the absence of other channels, the primary decay of HNLs to SM particles is hadronically [14, 15]. The mesons produced through these decays interact strongly with the protons and neutrons of the primordial plasma, thereby modifying the $p \leftrightarrow n$ conversion ratio which sets the primordial abundances. Most notably, the primordial abundance of ^{4}He, precisely measured as $Y_p = 0.2436 \pm 0.0038$ [16], would be mostly affected since most primordial neutrons and protons end up forming ^{4}He. Such considerations disfavour HNLs with masses $m_N \lesssim 1$ GeV, for small active-sterile mixing strengths required by current constraints and expected for light neutrino mass generation. Even lighter and longer-lived N are likewise disfavoured as they will act as additional degrees of freedom, or inject them through their decays, and may overclose the universe.

The above considerations apply for the minimal scenario where the HNL only couples via the active-sterile mixing. Instead, HNLs may also interact with an expanded exotic sector within specific beyond-the-SM scenarios. Often, these are high-scale scenarios where the HNL is charged under an additional gauge force, such as $B - L$ [17–21] and left-right-symmetric [19, 22–26] models. Less explored is the possibility of coupling the HNL to a lighter exotic sector. We here explore such a scenario where the HNL couples to a light, exotic pseudoscalar a, akin to an axion-like particle (ALP) [27–29]. We will refer to this dark scalar as ALP in the following, and it is dark in the sense that it couples only to the HNL in the first instance, with interactions to the SM suppressed by the active-sterile mixing and through loops.

Our motivation is to explore the cosmological consequences of changing the HNL decay width due to the additional channel $N \to a\nu$ in the scenario. While suppressed by both the active-sterile neutrino mixing and the ALP decay constant f_a, it is a two-body decay that can compete with the three-body (at parton level) decays to SM particles only. This will enlarge the region of interest constrained by BBN, i.e., where HNLs decay earlier and motivate direct searches under such an additional invisible HNL decay. At the same time, the production of ALPs and their own decays will themselves lead to constraints on the viable parameter space by ensuring the cosmological history, especially until the

time of the formation of the cosmic microwave background (CMB), is not affected. Any overabundance of ALPs would modify the expansion history of the Universe, either by also inducing a change on the primordial element abundances, if they are efficiently produced before BBN, or by increasing the temperature of the neutrino bath, if they decay strongly to active neutrinos before recombination. Furthermore, ALPs may be produced in the core of stars or supernovae, which leads to faster cooling and anomalous neutrino fluxes, posing additional constraints on strongly coupled ALPs.

The paper is organized as follows. In Sec. 2, we describe the model and determine the HNL and ALP decay widths as important quantities for our later considerations. In Sec. 3, we describe our modelling of the cosmological history in our scenario by setting up the Boltzmann equations which we separate into a regime before and after BBN. The relevant constraints from cosmology and astrophysics, as well as the expectations for direct searches, are then discussed in Sec. 4, and they are applied in Sec. 5 where we present our results in terms of the viable parameter space. Lastly we provide a conclusion and outlook in Sec. 6.

2 Model

In this work, we have extended the existing SM particle spectrum by adding a SM gauge singlet HNL and an ALP. The ALP only couples to the HNL in the unbroken SM and thus the mass of the ALP is not strictly tied to the QCD phase transition scale, Λ_{QCD}. In this extension, we outline a phenomenological framework which can describe the coupling between HNL and ALP and its implications for current phenomenological, cosmological and astrophysical constraints from other complimentary studies.

2.1 Lagrangian

In order to generate at least two non-degenerate active neutrino masses, as confirmed by the results from various neutrino oscillation experiments, it is necessary to introduce at least two HNLs. In general, we can extend the SM to include $\mathcal{N}$ HNLs as SM gauge-singlet Weyl fermion fields N_{iR} $(i = 1, .., \mathcal{N})$. Including a pseudoscalar ALP a that couples solely to N_{iR}, the most general and renormalisable Lagrangian is

$$\mathcal{L} = \mathcal{L}_{\text{SM}} + i\bar{N}_{iR}\slashed{\partial}N_{iR} - (Y_\nu)_{\alpha i}\bar{L}_\alpha \tilde{H} N_{iR} - \frac{1}{2}(\mathcal{M}_R)_{ij}\bar{N}^c_{iR}N_{jR} + \mathcal{L}_{aNN} + \text{h.c.} \qquad (2.1)$$

Here, $L_\alpha = (\nu_{\alpha L}, \ell_{\alpha L})^T$ and $H = (H^0, H^-)^T$ are the SM lepton and Higgs doublets, with flavour index $\alpha = e, \mu, \tau$ and $\tilde{H} \equiv i\sigma_2 H$ as the dual of H. Y_ν corresponds to the general complex Yukawa coupling matrix which couples N_{iR} to the SM spectrum. As HNLs are electromagnetically neutral and SM gauge-singlet particles, one can write a Majorana mass term where $\mathcal{M}_R$ corresponds to the lepton-number breaking scale. After electroweak symmetry breaking, the Higgs doublet acquires a vacuum expectation value $v/\sqrt{2} = \langle H \rangle$ which correspondingly generates the Dirac mass for neutrinos in the theory as $(\mathcal{M}_D)_{\alpha i} = (Y_\nu)_{\alpha i}\frac{v}{\sqrt{2}}$. The neutral fermion mass matrix can be written in the $(\nu^c_{\alpha L}, N_{jR})^T$

basis by a $(3 + \mathcal{N}) \times (3 + \mathcal{N})$ complex symmetric matrix as

$$\mathcal{M}_\nu = \begin{pmatrix} 0 & \mathcal{M}_D \\ \mathcal{M}_D^T & \mathcal{M}_R \end{pmatrix}, \tag{2.2}$$

where $\mathcal{M}_D$ and $\mathcal{M}_R$ are $3 \times \mathcal{N}$ and $\mathcal{N} \times \mathcal{N}$ matrices, respectively. We can consider $\mathcal{M}_R$ as diagonal without any loss of generality. One can introduce a $(3 + \mathcal{N}) \times (3 + \mathcal{N})$ unitary matrix,

$$U = \begin{pmatrix} U_{\nu\nu} & U_{\nu N} \\ U_{N\nu} & U_{NN} \end{pmatrix}, \tag{2.3}$$

which diagonalizes the matrix $\mathcal{M}_\nu$. $U_{\nu\nu}$ is related to the 3×3 Pontecorvo-Maki-Nakagawa-Sakata (PMNS) matrix, but may include non-unitary corrections due to the presence of $3 \times \mathcal{N}$ active-sterile mixing $U_{\nu N} = U_{N\nu} \equiv \mathcal{M}_D \mathcal{M}_R^{-1}$. Using this unitary matrix, the diagonalized neutral fermion mass matrix in the Majorana mass eigenbasis $(\nu_\lambda, N_\kappa)^T (\lambda = 1, 2, 3; \kappa = 1, .., \mathcal{N})$ will be

$$U^\dagger \mathcal{M}_\nu U^* = U^\dagger \cdot \begin{pmatrix} 0 & \mathcal{M}_D \\ \mathcal{M}_D^T & \mathcal{M}_R \end{pmatrix} \cdot U^* = \begin{pmatrix} (m_\nu)_{3\times 3} & 0 \\ 0 & (M_N)_{\mathcal{N}\times\mathcal{N}} \end{pmatrix}. \tag{2.4}$$

Here, m_ν and M_N are the diagonalized active and heavy neutrino masses, respectively. In the mass basis, the Majorana mass matrices can be written as

$$m_\nu \approx -\mathcal{M}_D \mathcal{M}_R^{-1} \mathcal{M}_D^T,$$
$$M_N \approx \mathcal{M}_R, \tag{2.5}$$

using the type-I seesaw approximation $\mathcal{M}_D \ll \mathcal{M}_R$.

In addition to the regular seesaw sector, we also assume that the ALPs a couples with the HNL N, but not with other SM particles directly. Hence, due to the pseudoscalar nature of ALPs, the Lagrangian for the ALP-HNL interaction is given by the derivative coupling [30] in the mass basis as

$$\mathcal{L}_{aNN} = \sum_{\kappa=1}^{\mathcal{N}} \frac{1}{f_a} (\partial_\mu a) \bar{N}_\kappa \gamma^\mu \gamma_5 N_\kappa = -\sum_{\kappa=1}^{\mathcal{N}} \frac{2i}{f_a} m_{N_\kappa} a \bar{N}_\kappa \gamma_5 N_\kappa, \tag{2.6}$$

where f_a is the ALP decay constant and m_{N_κ} are the eigenvalues of M_N. The second equality holds by applying the equation of motion for the HNLs and removing a total derivative after integration by parts [31]. Due to the small active-sterile mixing $U_{\nu N} = U_{N\nu} \equiv \sqrt{m_\nu M_N^{-1}}$, an interaction between the ALP and the active neutrinos ν_λ is induced. In the mass basis of the active neutrinos and HNLs, we can write the interaction Lagrangian between the ALP and active neutrinos as

$$\mathcal{L}_{a\nu\nu} = -\sum_{\lambda,\lambda'=1}^{3} \sum_{\kappa=1}^{\mathcal{N}} \frac{2i}{f_a} m_{N_\kappa} a (U_{\nu\nu}^\dagger U_{N\nu}^T)_{\kappa\lambda} (U_{N\nu}^* U_{\nu\nu})_{\kappa\lambda'} \bar{\nu}_\lambda \gamma_5 \nu_{\lambda'}$$

$$\approx -\sum_{\lambda,\lambda'=1}^{3} \frac{2i}{f_a} m_N a |U_{N\nu} U_{\nu\nu}^*|_{\lambda\lambda'}^2 \bar{\nu}_\lambda \gamma_5 \nu_{\lambda'} \tag{2.7}$$

where the second expression applies for (nearly) degenerate HNLs and λ, λ' denote the active neutrino mass eigenstates. Furthermore, the interaction Lagrangian for the $aN\nu$ vertex can be written similarly as

$$\mathcal{L}_{aN\nu} = -\sum_{\lambda'=1}^{3}\sum_{\kappa=1}^{\mathcal{N}} \frac{2i}{f_a} m_{N_\kappa} a (U^*_{N\nu} U_{\nu\nu})_{\kappa\lambda'} \bar{N}_\kappa \gamma_5 \nu_{\lambda'}. \tag{2.8}$$

While at least two HNLs are needed to explain all active neutrino masses and mixing, we are mainly interested in elucidating the principle effects in our framework. For simplicity, by considering a single HNL, $N_1 \equiv N$, we can acquire all the important information from the framework using this simplified viewpoint. Furthermore, we consider the active-sterile mixing of N_1 with a single active neutrino ν_1 which is mostly electron-type neutrino i.e., $\nu_1 \equiv \nu_e$, without loss of generality. From now on, we take $|U_{\nu\nu}|^2 \sim \mathcal{O}(1) \gg |U_{\nu N}|^2 = |U_{N\nu}|^2$ and $U_{\nu N} = U_{eN}$. Equations (2.6) and (2.7) then take the form

$$\mathcal{L}_{aNN} = -\frac{2i}{f_a} m_N a \bar{N} \gamma_5 N,$$

$$\mathcal{L}_{aN\nu} = -\frac{2i}{f_a} m_N U_{eN} a \bar{N} \gamma_5 \nu_e,$$

$$\mathcal{L}_{a\nu\nu} = -\frac{2i}{f_a} m_N |U_{eN}|^2 a \bar{\nu}_e \gamma_5 \nu_e = -\frac{2i}{f_a} m_\nu a \bar{\nu}_e \gamma_5 \nu_e, \tag{2.9}$$

with the light neutrino mass $m_\nu = |U_{eN}|^2 m_N$ induced by the seesaw mechanism.

2.2 HNL decays

A Majorana HNL with a mass of a few hundred MeV to GeV decays via various channels into SM particles. All these decays are four-fermion interactions mediated by either a Z or W boson. We will briefly discuss these SM decay channels of HNLs here with a detailed discussion found in [14, 15]. In our framework with only one HNL species that couples with the first generation only, we have the corresponding decay channels of HNLs as:

$N \to \nu_e \ell^- \ell^+$: mediated by charged (for $\ell = e$) and neutral currents (for $\ell = e, \mu, \tau$). The corresponding decay width is (with $x_\ell = m_\ell/m_N$)

$$\Gamma^{\nu_e \ell^- \ell^+} = |U_{eN}|^2 \frac{G_F^2 m_N^5}{96\pi^3} \left[\left(C_1 + 2\sin^2\theta_W \delta_{e,\ell} \right) f_1(x_\ell) + \left(C_2 + \sin^2\theta_W \delta_{e,\ell} \right) f_2(x_\ell) \right], \tag{2.10}$$

with

$$C_1 = \frac{1}{4}(1 - 4\sin^2\theta_W + 8\sin^4\theta_W), \qquad C_2 = \frac{1}{2}(-\sin^2\theta_W + 2\sin^4\theta_W), \tag{2.11}$$

and the functions are defined as

$$f_1(x) = (1 - 14x^2 - 2x^4 - 12x^6)\sqrt{1 - 4x^2} + 12x^4(x^4 - 1)L(x)$$

$$f_2(x) = 4\left[x^2(2 + 10x^2 - 12x^4)\sqrt{1 - 4x^2} + 6x^4(1 - 2x^2 + 2x^4)L(x) \right], \tag{2.12}$$

with

$$L(x) = \ln\left[\frac{1 - 3x^2 - (1 - x^2)\sqrt{1 - 4x^2}}{x^2(1 + \sqrt{1 - 4x^2})} \right]. \tag{2.13}$$

$N \to e^- \ell^+ \nu_\ell$: mediated by a charged current with $\ell = \mu, \tau$. The decay width for this process is

$$\Gamma^{e^- \ell^+ \nu_\ell} = |U_{eN}|^2 \frac{G_F^2 m_N^5}{192\pi^3} \left[1 - 8x_\ell^2 + 8x_\ell^6 - x_\ell^8 - 12x_\ell^4 \ln(x_\ell^2) \right]. \tag{2.14}$$

$N \to \nu_e \nu_\ell \bar{\nu}_\ell$: mediated by a neutral current with $\ell = e, \mu, \tau$. The decay width can be written as

$$\Gamma^{\nu_e \nu_\ell \bar{\nu}_\ell} = \frac{G_F^2}{96\pi^3} |U_{eN}|^2 m_N^5. \tag{2.15}$$

$N \to P\nu_e$: with a neutral pseudoscalar meson $P = \pi^0, K^0, \eta, \eta'$. The decay width is

$$\Gamma^{P\nu_e} = \frac{G_F^2 m_N^3}{32\pi} f_P^2 |U_{eN}|^2 (1 - x_P^2)^2, \tag{2.16}$$

with the meson decay constant f_P whose values we have taken from [15] and $x_P = m_P/m_N$.

$N \to P^+ e^-$: with a charged pseudoscalar meson $P^+ = \pi^+, K^+, D^+, D_s^+$. The decay width is

$$\Gamma^{P^+ e^-} = \frac{G_F^2 m_N^3}{16\pi} f_P^2 |U_{eN}|^2 |V_{qq'}|^2 \lambda^{1/2}(1, x_P^2, x_e^2) \left[1 - x_P^2 - x_e^2(2 + x_P^2 - x_e^2) \right]. \tag{2.17}$$

where $V_{qq'}$ denotes the CKM mixing matrix element involving relevant quarks in the produced meson and $\lambda(a, b, c) \equiv (a - b - c)^2 - 4bc$.

$N \to V\nu_e$: with a neutral vector meson $V = \rho, \omega, \phi, K^{*0}$. The decay width can be written as

$$\Gamma^{V\nu_e} = \frac{G_F^2 m_N^3}{32\pi m_V^2} f_V^2 \kappa_V^2 |U_{eN}|^2 (1 + 2x_V^2)(1 - x_V^2)^2. \tag{2.18}$$

where f_V and κ_V represent the decay constant and the vector coupling associated with the produced neutral vector mesons, respectively.

$N \to V^+ e^-$: with a charged vector meson $V^+ = \rho^+, K^{*,+}$. The decay width can be written as

$$\Gamma^{V^+ e^-} = \frac{G_F^2 m_N^3}{16\pi m_{V^\pm}^2} f_V^2 |U_{eN}|^2 |V_{qq'}|^2 \lambda^{1/2}(1, x_V^2, x_e^2) \left[(1 - x_V^2)(1 + 2x_V^2) + x_e^2(x_V^2 + x_e^2 - 2) \right]. \tag{2.19}$$

The total decay width for a Majorana HNL decaying into purely SM particles is then

$$\Gamma^{N \to \text{SM}} = \sum_\ell \Gamma^{\nu_e \ell^- \ell^+} + \sum_{\ell = \mu, \tau} 2\Gamma^{e^- \ell^+ \nu_\ell} + \sum_\ell \Gamma^{\nu_e \nu_\ell \bar{\nu}_\ell}$$
$$+ \sum_P \Gamma^{P\nu_e} + \sum_P 2\Gamma^{P^+ e^-} + \sum_V \Gamma^{V\nu_e} + \sum_V 2\Gamma^{V^+ e^-}. \tag{2.20}$$

The factors of two are due to the Majorana HNL decaying into opposite charge combinations, e.g., $\Gamma^{P^- e^+} = \Gamma^{P^+ e^-}$.
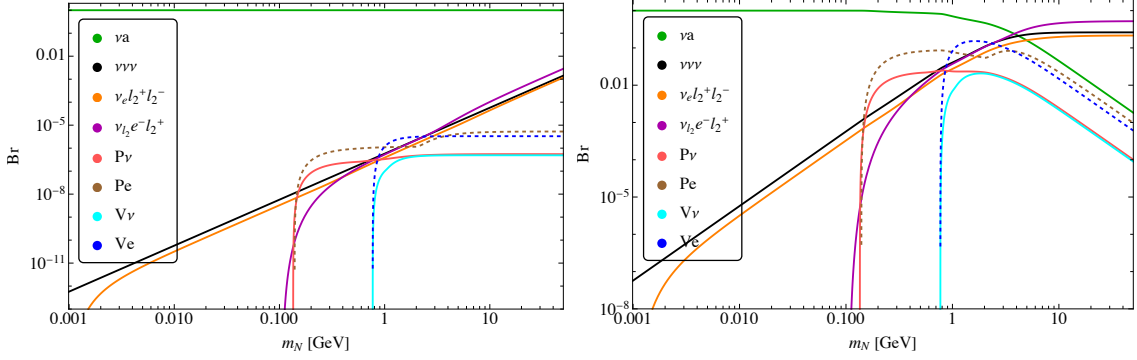
Figure 1. Branching ratios of HNL as a function of the HNL mass m_N for an ALP mass $m_a = 1$ keV, and decay constant $f_a = 1$ TeV (left panel) and $f_a = 10^{2.5}$ TeV (right panel).

Due to the interaction in Eq. (2.9), a new decay channel for HNLs is also possible, where the HNL decays as $N \to a\nu$ via the active-sterile mixing at tree level. The decay width, in the limit where $m_\nu \ll m_N$, can be written as

$$\Gamma^{N \to a\nu} = \frac{|U_{eN}|^2 m_N^3}{4\pi f_a^2} \sqrt{1 + \left(\frac{m_a}{m_N}\right)^2} \left[1 - \left(\frac{m_a}{m_N}\right)^2\right]^{3/2} \approx \frac{|U_{eN}|^2 m_N^3}{4\pi f_a^2}, \tag{2.21}$$

where the last equality holds in the limit where $m_a, m_\nu \ll m_N$. Hence the lifetime of the HNL considering only this decay mode, calculated in its rest frame, can be expressed as

$$\tau_{N \to a\nu} \approx 8.6 \times 10^{-4} \text{ s} \times \left(\frac{f_a}{1 \text{ TeV}}\right)^2 \times \left(\frac{10^{-14}}{|U_{eN}|^2}\right) \times \left(\frac{1 \text{ GeV}}{m_N}\right)^3. \tag{2.22}$$

The total HNL decay width to SM particles can be approximately written as [9]

$$\Gamma^{N \to \text{SM}} \approx \left(30 \, \Gamma^{2-\text{body}} + 10 \, \Gamma^{3-\text{body}}\right) |U_{eN}|^2$$
$$\approx \left(\frac{6 f_M^2}{\pi} + \frac{m_N^2}{20\pi^3}\right) m_N^3 |U_{eN}|^2 G_F^2, \tag{2.23}$$

where $f_M \approx \mathcal{O}(0.1)$ GeV corresponds to the typical decay constant of the produced pseudoscalar or vector meson. Comparing this with Eq. (2.21), it is clear that the $N \to a\nu$ channel will be dominant if

$$m_N < \frac{\sqrt{5|1 - 24 G_F^2 f_M^2 f_a^2|\pi}}{f_a G_F}, \tag{2.24}$$

independent of $|U_{eN}|^2$.

The branching ratios of the HNL decaying to various particles as a function of mass of the HNL for two different values of f_a are shown in Fig. 1. In this work, as we are mostly interested in the regime where $m_a \ll m_N$, correspondingly we have chosen $m_a = 1$ keV and varied $m_N \in [10^{-3} - 50]$ GeV range. In the left panel, we have considered $f_a = 1$ TeV where the Br($N \to a\nu$) $\approx 100\%$ (solid green) throughout the entire mass range of HNL,
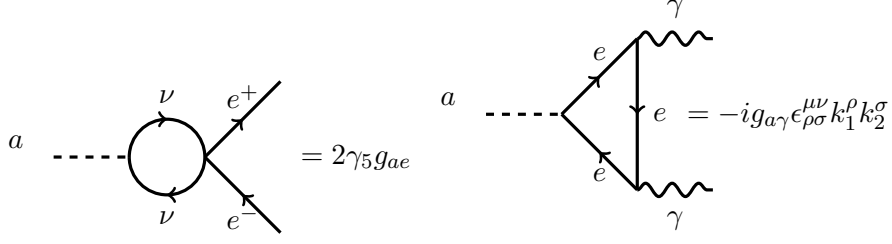
Figure 2. Effective couplings of the ALP to electrons (left) and photons (right).

while the behaviour of different SM decay channels are shown as, $N \to \nu\nu\nu$ (solid black), $N \to \nu_e(e^+e^- + \mu^+\mu^- + \tau^+\tau^-)$ (solid orange), $N \to e^-(\nu_\mu\mu^+ + \nu_\tau\tau^+)$ (solid magenta), different pseudoscalar (P) and vector (V) mesonic channels (which become relevant for $m_N \geq m_\pi$) as $N \to P\nu$ (solid red), $N \to Pe$ (dashed brown), $N \to V\nu$ (solid cyan), $N \to Ve$ (dashed blue). In the right panel of the figure we have taken $f_a = 10^{2.5}$ TeV, for which the coupling of the ALP to HNL significantly decreases. Here, for lower mass of HNL the axionic decay channel still dominates the scenario, as expected from eq. (2.24), while for $m_N > m_\pi$, as the mesonic channels come into picture, the branching ratio to axionic channel drops significantly as compared to the SM decay channels.

2.3 ALP decays

The interaction between the ALPs and active neutrinos in eq. (2.7) causes the ALP to decay. This decay channel occurs at tree level, thus dominating the ALP decay width, and it is given by

$$\Gamma^{a \to \nu\nu} = \frac{1}{f_a^2}\frac{m_N^2 m_a U_{eN}^4}{2\pi}\sqrt{1 - \frac{4m_\nu^2}{m_a^2}}\left(1 - \frac{2m_\nu^2}{m_a^2}\right) \simeq \frac{m_N^2 m_a U_{eN}^4}{2\pi f_a^2} \qquad (2.25)$$

where we have considered $m_a \gg m_\nu$ to arrive at the last expression.

No other decay channels are available at tree level. However, as it will be seen below (see section 4), most of the constraints on axion-like particles come from their interactions with electrons and photons. Though the Lagrangian in eq. (2.9) does not produce axion-electron or axion-photon interactions at tree level, such couplings can be induced at 1-loop and 2-loop respectively, as shown in Figure 2.

These effective axion-electron and axion-photon couplings, g_{ae} and $g_{a\gamma}$, can cause the ALP to decay to a pair of electrons or photons and, in the limit where $m_a, m_\nu, m_e \ll m_N$, are given by

$$g_{ae} \approx \frac{\sqrt{2}G_F g_{aN}|U_{eN}|^4 m_e m_N}{16\pi^2} = \frac{\sqrt{2}G_F |U_{eN}|^4 m_e m_N^2}{16\pi^2 f_a},$$

$$g_{a\gamma} \approx \frac{e^2 g_{ae}}{2\pi^2 m_e}\left(1 + \frac{1}{12}\frac{m_a^2}{m_e^2}\right) = \frac{\sqrt{2}e^2 G_F |U_{eN}|^4 m_N^2}{32\pi^4 f_a}\left(1 + \frac{1}{12}\frac{m_a^2}{m_e^2}\right), \qquad (2.26)$$

where $g_{aN} = m_N/f_a$.

Scenario	m_N [GeV]	$|U_{eN}|^2$	f_a [TeV]	m_a [keV]
1	10^{-1}	10^{-10}	1	1
2	$10^{-0.4}$	$10^{-9.2}$	$10^{2.5}$	1
3	-	-	1	10^{-2}
4	-	-	$10^{2.5}$	10^{-2}

Table 1. Benchmark scenarios labelled by the red squares on Fig.5. For fixed ALP mass $m_a = 1$ keV, they are $m_N = 10^{-1}$ GeV and $|U_{eN}|^2 = 10^{-10}$ for $f_a = 1$ TeV and $m_N = 10^{-0.4}$ GeV and $|U_{eN}|^2 = 10^{-9.2}$ for $f_a = 10^{2.5}$ TeV respectively. The last two scenarios are given at fixed $m_a = 10$ eV for $f_a = 1$ TeV and $f_a = 10^{2.5}$ TeV, respectively.

Nevertheless, for light ALPs, $m_a \lesssim 1$ keV, which is the focus of this study, the only open decay channels for the ALPs are either a pair of active neutrinos or a pair of photons. But, as seen in Fig. 2, the diphoton decay happens at 2-loop and thus it is significantly suppressed with respect to the decay to active neutrinos. For example, the decay width to photons of a 1 keV ALP with decay constant of 1 TeV will be of order 10^{-46} GeV, negligible compared to decay width to active neutrinos in eq. (2.25).

The ALP lifetime can thus be computed from its decay width to two active neutrinos. So in ALP rest frame,

$$\tau_a = 1 \text{ sec} \times \left(\frac{1 \text{ GeV}}{m_N}\right)^2 \times \left(\frac{1 \text{ keV}}{m_a}\right) \times \left(\frac{2.03 \times 10^{-6}}{|U_{eN}|^2}\right)^2 \times \left(\frac{f_a}{1 \text{ TeV}}\right)^2. \tag{2.27}$$

For HNLs and ALPs in the mass range of interest, $m_N \sim 1$ GeV and $m_a \sim 1$ keV, the lifetime of the ALPs, and hence the scenario that is realised, depends on the ALP-HNL interaction $1/f_a$ and the active-sterile mixing U_{eN}. For example, an ALP that is stable compared to the age of the universe (i.e., $\tau_a > 10^{17}$ sec) and $f_a \sim 1$ TeV would require $|U_{eN}|^2 \leq 10^{-14.2}$.

2.4 Benchmark Scenarios

There are four benchmark points we choose to study are given in Tab. 1. The allowed parameter space is investigated for all four scenarios in active-HNL mixing versus HNL mass planes in Sec. 5. The number density evolutions and interaction rates are studied explicitly through cosmological history for scenarios 1 and 2 as examples. These benchmark points satisfy the requirements that HNL decays before the start of BBN and ALP decays before the start of CMB. The reason for these choice is explained in Sec. 3 and the points are also deliberately chosen in (or close to) the seesaw region in order to explain the masses of active neutrinos.

3 Cosmological history of HNLs and ALPs

In the hot dense plasma of the early Universe, it is expected that the interactions between the HNLs and SM particles are strong enough to maintain thermal and chemical equilibrium
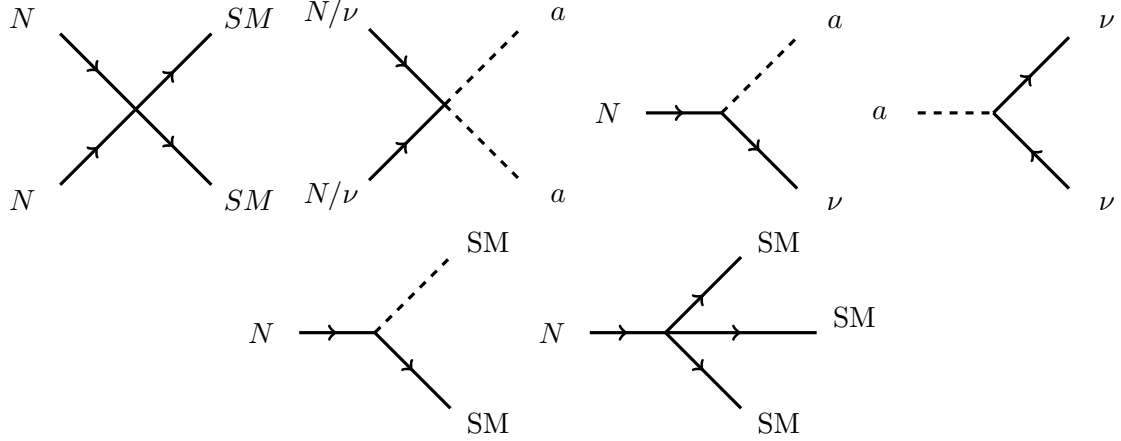
Figure 3. Relevant processes for the scattering and decay of HNLs, ALPs and SM particles, responsible for determining their abundances. The diagrams on the left describe the scattering of HNLs with SM particles ($NN \leftrightarrow$ SM), and the scattering of HNLs or active neutrinos with ALPs ($NN \leftrightarrow aa$). The diagrams on the right and second row depict the decays of HNLs ($N \to a\nu$ and $N \to$ SM) and ALPs ($a \to \nu\nu$).

between the two sectors. HNLs with masses around the GeV scale typically do not have time to freeze-out as their decays into SM particles, and in our framework into ALPs, will deplete their abundance sufficiently fast. On the other hand, the interactions of HNLs and SM particles with ALPs are typically weak, and hence we assume that ALPs do not start in thermal equilibrium with the SM and HNLs, and that their initial abundance is negligible (freeze-in production). The scattering between ALPs and HNLs might briefly bring the ALPs in thermal equilibrium, for small enough f_a, but they would soon freeze out, and eventually decay into active neutrinos. All of these decay channels and scattering rates play an important role in the evolution of the energy and number densities of HNLs and ALPs throughout the history of the universe. The most relevant processes that determine the abundances of HNLs and ALPs can be seen in Fig.3.

The change on the energy and number densities of the various particle species due to the expansion of the universe and the processes in Fig. 3 can be computed with the Boltzmann equations [32, 33]

$$\frac{d\rho_X}{dt} + 3H(\rho_X + p_X) = \frac{\delta\rho_X}{\delta t} = \int g_X E \frac{d^3p}{(2\pi)^3} \mathcal{C}[f],$$

$$\frac{dn_X}{dt} + 3Hn_X = \frac{\delta n_X}{\delta t} = \int g_X \frac{d^3p}{(2\pi)^3} \mathcal{C}[f], \qquad (3.1)$$

where ρ_X, p_X and n_X are energy density, pressure and number density of particle X, H the Hubble parameter, g_X its internal degrees of freedom and $\delta\rho_X/\delta t$ and $\delta n_X/\delta t$ the energy and number density transfer rates, computed with the collision operator $\mathcal{C}[f]$, which takes into account all energy and number changing processes.

The transfer rates, $\delta\rho_X/\delta t$ and $\delta n_X/\delta t$, can be obtained by calculating the thermally averaged cross sections and decay rates for each process where the species X is involved,

$\langle \sigma_{X \to Y} v \rangle$ and $\langle \Gamma_{X \to Y} \rangle$. A useful quantity is the thermally averaged interaction density $\gamma_{X \to Y}$, defined as

$$\gamma_{X \to Y} = \langle \sigma_{X \to Y} v \rangle n_X^{eq,2} = \langle \Gamma_{X \to Y} \rangle n_X^{eq}, \tag{3.2}$$

where n_X^{eq} is the number density of species X while on thermal equilibrium. The thermally averaged decay width density is defined as

$$\gamma_{X \to Y_1 \cdots} = n_X^{eq}(z) \frac{K_1(z)}{K_2(z)} \Gamma_X, \tag{3.3}$$

with $z = \frac{m_X}{T}$, Γ_X is the zero-temperature decay width of particle X, and $K_{1(2)}(z)$ are the Bessel function of first (second) kind. The thermally averaged cross-section density is calculated as,

$$\gamma_{X_1 X_2 \leftrightarrow Y_1 Y_2} = \frac{T}{64\pi^4} \int_{s_{\min}}^{\infty} s^{1/2} \hat{\sigma}(s) \mathrm{K}_1 \left(\frac{\sqrt{s}}{T} \right) ds, \tag{3.4}$$

where $\hat{\sigma}(s) = 2s\sigma(s)\lambda(1, m_{X_1}^2/s, m_{X_2}^2/s)$ is the reduced cross-section, with the function $\lambda(a,b,c) = (a - b - c)^2 - 4bc$, and the minimal value of the integral is defined as $s_{min} = \mathrm{Max}[(m_{X_1} + m_{X_2})^2, (m_{Y_1} + m_{Y_2})^2]$.

The addition of the ALPs to this model has the intended consequence of forcing the HNLs to decay faster than in vanilla HNL models. Consequently, even for HNL masses of the order of $10 - 100$ MeV, HNLs decay fast enough to avoid affecting the BBN abundances. In contrast, the ALPs should not decay before BBN, otherwise they would in turn modify the primordial abundances. Therefore, we study the HNL and ALP abundances in two different time epochs, before BBN and between BBN and recombination[1]. After recombination the ALPs may or may not be stable, and that will have some astrophysical consequences that will discussed in Section 4.

3.1 Abundances before BBN

We start by assuming that after some inflationary epoch and subsequent reheating, the SM particles are in equilibrium in the early Universe. The actual value of the reheating temperature is no importance, since most particles will be at their equilibrium densities, but it must be low enough to ensure that the ALPs are not strongly coupled after reheating. The HNLs are thus assumed to be in thermal and kinematical equilibrium with the SM, but the ALPs are not. The evolution of the densities of HNL and ALP can be described by coupled Boltzmann equations, as in eq. (3.1). Before neutrino decoupling, the HNL number density is given by

$$\begin{aligned} \frac{dn_N}{dt} + 3Hn_N = &- \langle \sigma_{NN \to SM} \, v \rangle \left(n_N^2 - n_N^{\mathrm{eq},2} \right) - \langle \sigma_{NN \to aa} \, v \rangle \left(n_N^2 - n_N^{\mathrm{eq},2} \frac{n_a^2}{n_a^{\mathrm{eq},2}} \right) \\ &- \langle \Gamma_{N \to SM} \rangle \left(n_N - n_N^{\mathrm{eq}} \right) - \langle \Gamma_{N \to a\nu} \rangle \left(n_N - n_N^{\mathrm{eq}} \frac{n_a}{n_a^{\mathrm{eq}}} \right), \end{aligned} \tag{3.5}$$

---

[1]We should mention that we here consider the onset of BBN to occur at the time of neutrino decoupling, i.e. $t \sim 1$ s. This approximation holds as long as none of the number changing processes involved are active between that time and the end of BBN, $t \sim 10^4$ s.

where $\langle \sigma_{NN \to \text{SM}} v \rangle$, $\langle \sigma_{NN \to aa} v \rangle$, $\langle \Gamma_{N \to \text{SM}} \rangle$ and $\langle \Gamma_{N \to a\nu} \rangle$ are the thermally-averaged scattering cross-sections of HNL annihilation to SM particles and ALPs, and the thermally-averaged decay widths of HNLs into light SM particles and ALP-active neutrino pair, respectively. Similarly the Boltzmann equation for ALPs is

$$\frac{dn_a}{dt} + 3Hn_a = -\langle \sigma_{aa \to \nu\nu} \; v \rangle \left(n_a^2 - n_a^{\text{eq},2} \right) - \langle \sigma_{aa \to NN} \; v \rangle \left(n_a^2 - n_a^{\text{eq},2} \frac{n_N^2}{n_N^{\text{eq},2}} \right)$$
$$- \langle \Gamma_{a \to \nu\nu} \rangle \left(n_a - n_a^{\text{eq}} \right) + \langle \Gamma_{N \to a\nu} \rangle \left(n_N - n_N^{\text{eq}} \frac{n_a}{n_a^{\text{eq}}} \right), \tag{3.6}$$

which also contains various contributions from the scattering of ALPs with the HNLs and neutrinos and the thermally averaged ALP decay width $\langle \Gamma_{a \to \nu\nu} \rangle$. The solution of these Boltzmann equations will give the evolution of the number densities of HNLs and ALPs between some unspecified reheating time and the time of neutrino decoupling, $t \sim 1$ s. To solve the Boltzmann equations we make a variable transformation, to the comoving yield $Y_X = n_X/s$ for any species X, where s is the entropy density given by

$$s = \frac{2\pi^2}{45} g_* T^3. \tag{3.7}$$

where g_* is the number of relativistic degrees of freedom and T the temperature of the thermal bath of SM particles. The Boltzmann equations for the yield Y_X, using the more useful thermally averaged densities $\gamma_{X \to Y}$, can therefore be written as

$$zHs\frac{dY_N}{dz} = -\gamma_{NN \to SM}^{\text{eq}} \left(\frac{Y_N^2}{Y_N^{\text{eq},2}} - 1 \right) + \gamma_{aa \to NN}^{\text{eq}} \left(\frac{Y_a^2}{Y_a^{\text{eq},2}} - \frac{Y_N^2}{Y_N^{\text{eq},2}} \right)$$
$$- \gamma_{N \to SM} \left(\frac{Y_N}{Y_N^{\text{eq}}} - 1 \right) - \gamma_{N \to a\nu} \left(\frac{Y_N}{Y_N^{\text{eq}}} - \frac{Y_a}{Y_a^{\text{eq}}} \right), \tag{3.8}$$

$$zHs\frac{dY_a}{dz} = -\gamma_{aa \to \nu\nu}^{\text{eq}} \left(\frac{Y_a^2}{Y_a^{\text{eq},2}} - 1 \right) - \gamma_{aa \to NN}^{\text{eq}} \left(\frac{Y_a^2}{Y_a^{\text{eq},2}} - \frac{Y_N^2}{Y_N^{\text{eq},2}} \right)$$
$$- \gamma_{a \to \nu\nu} \left(\frac{Y_a}{Y_a^{\text{eq}}} - 1 \right) + \gamma_{N \to a\nu} \left(\frac{Y_N}{Y_N^{\text{eq}}} - \frac{Y_a}{Y_a^{\text{eq}}} \right), \tag{3.9}$$

with $z = m_N/T$.

3.2 Abundance of ALPs after BBN and temperature evolution

As we saw before, in all scenarios we consider, the abundance of HNLs depletes very fast before BBN. As a consequence, the main production mechanisms for ALPs, which were HNL-ALP scattering and HNL decays, are really inefficient after BBN and thus the ALP abundance only decreases at late times. Even the processes $aa \leftrightarrow N\nu$ and $aa \leftrightarrow \nu\nu$ fall out of thermal equilibrium significantly before BBN, as seen below in Fig. 4. Therefore, the abundance of ALPs after the end of BBN is solely determined by their decays. Their Boltzmann equation is therefore given by[12]

$$zHs\frac{dY_a}{dz} = -\gamma_{a \to \nu\nu} \left(\frac{Y_a}{Y_a^{\text{eq}}} - 1 \right) \qquad \text{with z} > \text{z}_{\text{BBN}}. \tag{3.10}$$

If the ALP decays are fast enough, as in the left-hand panel of Figure 4, the ALPs decay shortly after the end of BBN, and their number density completely disappears. Conversely, the abundance of long-lived ALPs becomes frozen-out after BBN, and will only deplete slowly, depending on their lifetime.

Before neutrino decoupling, the temperatures of the photon and neutrino baths evolved together, changing only via adiabatic cooling since ALP decays are negligible before BBN [34]. After the end of BBN, however, the decays of ALPs to neutrinos, $a \to \nu\nu$ become relevant, which will introduce energy into the neutrino bath and thus increase its temperature. An increase on the neutrino temperature relative with the photon temperature at the time of recombination has a strong impact on the number of effective neutrino degrees of freedom N_{eff}. Because of this, we need to track separately the evolution of the photon and neutrino temperatures from the end of BBN until the formation of the CMB. Neglecting chemical potentials and effects from neutrino oscillations, the evolution of the temperatures with time is given by [33, 35]

$$\frac{dT_\gamma}{dt} = -\frac{4H\rho_\gamma + 3H(\rho_e + p_e)}{\frac{\partial\rho_\gamma}{\partial T_\gamma} + \frac{\partial\rho_e}{\partial T_\gamma}}$$
$$\frac{dT_\nu}{dt} = -\frac{12H\rho_\nu + 3H(\rho_a + p_a) + \delta\rho_a/\delta t}{3\frac{\partial\rho_\nu}{\partial T_\nu} + \frac{\partial\rho_a}{\partial T_\nu}} \tag{3.11}$$

where ρ_i and p_i are the energy density and pressure of particle species i, and $\delta\rho_a/\delta t$ is the energy exchange rate from ALPs to neutrinos, given by the collision operator in eq.(3.1). Equation (3.11) takes into account the decoupling of the electrons from the photon bath when they become non-relativistic, as well as the decoupling of the ALP from the neutrino bath when $T_\nu \gtrsim m_a$.

3.3 Abundance and interaction rate evolution

Fig. 4 shows the evolution of the thermally averaged scattering and decay rates (top row) and the number density of various species (bottom row) for two different scenarios from Table 1. Scenario 1 has $m_N = 10^{-1}$ GeV, $|U_{eN}|^2 = 10^{-10}$, $f_a = 1$ TeV and $m_a = 1$ keV. Scenario 2 has $m_N = 10^{-0.4}$ GeV, $|U_{eN}|^2 = 10^{-9.2}$, $f_a = 10^{2.5}$ TeV and $m_a = 1$ keV.

The rate evolution plots show how the various rates evolve compared to the Hubble parameter (red). In scenario 1, shown on the left, the thermally averaged scattering rate $aa \to NN$ (solid blue) becomes efficient for a short period of time at around $z \sim 1$, which brings the ALPs and HNLs close to thermal equilibrium. Other scattering rates, such as $aa \to \nu\nu$, with either N (dotted blue) or ν (dashed blue) mediation, are negligible. Once the ALP-HNL scattering rate becomes inefficient shortly before the onset of BBN, HNL decaying to ALPs (green) become the primary source of ALP production while the HNLs are abundant enough. Other HNL decays to SM particles (orange) only become efficient in scenario 1 much after all HNLs have decayed away to ALPs, and thus have no effect on the evolution. Lastly, a long time after BBN, but before recombination, the decays of ALPs, $a \to \nu\nu$ (pink) become efficient and make the ALPs decay completely before the formation of the CMB. On the other hand, in scenario 2 on the right, the scattering rates are never
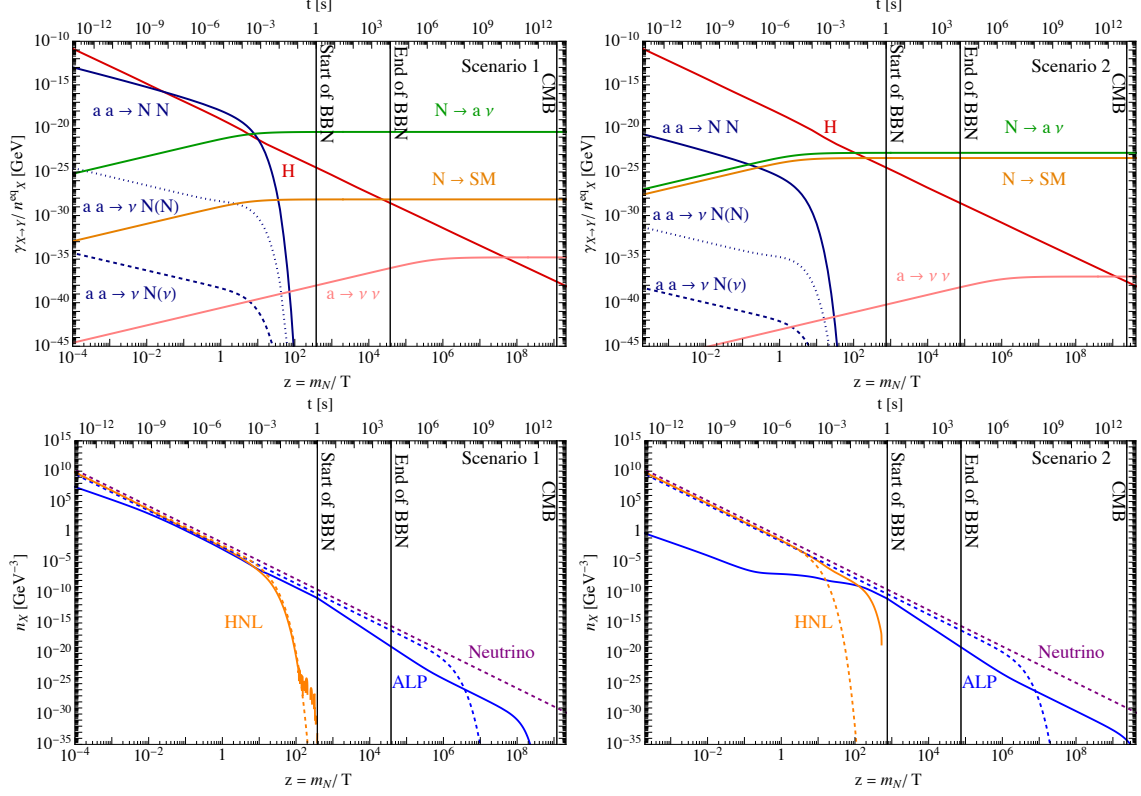
Figure 4. Evolution plots of the thermally averaged scattering and decay rates (top) and number densities (bottom), with $z = m_N/T$ and time, for benchmark scenarios 1 (left) and 2 (right) from Tab. 1. The scattering rates of ALPs with HNLs and neutrinos (blue) are shown in the top row compared to the evolution of the Hubble rate (red), along with the decay rates of HNLs to SM particles (orange) and ALPs (green) and the decay rate of the ALPs (pink). The bottom row shows the number density of ALPs (blue) in and out of equilibrium (dashed and solid respectively), as well as the number densities of HNLs (orange) and neutrinos (purple).

efficient enough, so the HNLs and ALPs are never in thermal equilibrium. The decay of HNLs to ALPs (green) is thus the only source of ALP production, but in this scenario it is comparable to the HNLs decays to SM particles (orange), and thus not all HNLs decay to ALPs. Since the ALP-neutrino interaction rate is weaker compared to scenario 1, due to larger f_a, ALPs do not decay efficiently in scenario 2, as their decay rate only becomes efficient around or after the formation of the CMB, which causes the ALPs to survive after recombination.

In the number density plots in the bottom row, the orange curves show the actual (solid) and equilibrium (dashed) number density for HNL, the blue curves show the actual (solid) and equilibrium (dashed) number density for ALP and the dashed purple curve gives the equilibrium density for neutrinos. In scenario 1, the strong scattering between HNLs and ALPs brings them close to thermal equilibrium at around $z \sim 1$. Shortly after, the HNLs become non-relativistic and thus their actual and equilibrium abundances are Boltzmann suppressed, thereby falling rapidly before BBN. Since the ALPs and HNLs are

close to equilibrium already, the increasing effect of HNL decays on the ALP abundance is small, and in fact causes the ALP abundance to decrease as inverse decays tend to dominate when the ALP population is high. Lastly, after BBN the ALPs become non-relativistic, but initially there are no equilibrium processes that can deplete their abundance, and thus they freeze-out, i.e. their real abundance (solid blue) overshoots their equilibrium abundance (dashed blue). Finally, shortly before recombination, ALPs decay to light neutrinos, depleting their abundance completely. In scenario 2, the ALPs are never in thermal equilibrium, and are only efficiently produced by HNL decays, so they freeze-in after the HNLs become non-relativistic and disappear. In this scenario, ALPs are longer lived, and thus their abundance freezes-out, as before, but only depletes slowly before the formation of the CMB.

4 Constraints from cosmology, astrophysics and direct searches

In this work we have introduced two new particles, a HNL and an ALP that modify very significantly the evolution of the early Universe compared to ΛCDM. The cosmological and astrophysical implications of both of these species are well known separately [27, 36, 37]. However, their combination has a somewhat different effect, as the HNLs are allowed to be lighter than in most previous scenarios, due to the weakening of the BBN bound (see below), and also due to the ALPs coupling exclusively to neutrinos via the HNL portal. Consequently we need to evaluate the predictions of our model towards known cosmological and astrophysical observables and hence assess whether their strong constraints render the model invalid or there are still parameter combinations that are unconstrained. For this purpose we study how this model affects the formation of primordial elements (BBN), the observations of the CMB, as well as astrophysical constraints such as those from the observation of the supernova SN1987A, and others such as extra-galactic background light (EBL) or X-ray constraints. Additionally, the new decay channel for HNLs available in this model modifies the prospects of direct searches for HNLs at colliders, fixed target or beam dump experiments. Consequently, we also study the sensitivity of our model to direct searches for HNLs at future facilities.

4.1 Big Bang Nucleosynthesis

The predictions of ΛCDM with regards to the formation of the primordial elements match very well with their observed present abundances[2] [40, 41]. These predictions are, however very sensitive to the cosmological state of the Universe at any time between neutrino decoupling and the CMB. Any modification of the temperature of neutrino decoupling, the rate of expansion of the Universe or energy injection in the primordial plasma, may cause a catastrophic change on the formation of light elements. This is specially true in our scenario, where the decays of HNLs into mesons disturb the $p \leftrightarrow n$ conversion

---

[2]The present-day abundance of ^7Li is currently in disagreement with the predictions from standard cosmology. Attempts have been made to provide an explanation in modified cosmologies, with varying degrees of success [38, 39]. Therefore, it remains unclear whether this is caused by modifications over ΛCDM or an inaccurate measurement of their present abundance.

processes that set the initial proton and neutron abundances for BBN [42]. If the HNLs decay fast enough, however, the abundances of protons and neutrons have time to restore to the expected values from ΛCDM, and thus there is no effect on BBN. Hence, we set a conservative limit on the HNL lifetime of $\tau_N < 0.023$ s [42], beyond which the decays will disturb the BBN abundances too much and is therefore marked as excluded in our scenario.

In addition to the decays of the HNLs, the decays of ALPs may also modify the primordial plasma and affect BBN. If the ALPs decay before neutrino decoupling, since their primary decay channel is $a \to \nu\nu$, they would modify the neutrino spectrum and increase the temperature of the neutrino bath, thereby delaying neutrino decoupling and the formation of primordial elements. Consequently, we do not consider scenarios where the ALPs have short lifetimes, and to ensure that they do not directly affect BBN, we only consider ALPs decaying after the end of BBN, i.e $\tau_a > 10^4$ s. Subsequent decays of the ALPs may also dissociate the formed elements and modify their abundance [34], however this dissociation is mostly caused by electromagnetic cascades, which are rare in our scenario since the decay rate of $a \to \gamma\gamma$ is negligible.

Even if the ALPs do not decay before BBN, they may still affect the formation of the primordial elements if they are too abundant. Since ALPs are relativistic before neutrino decoupling, a sufficient abundance would act as dark radiation and thus modify the Hubble rate during radiation domination. This effect can be understood as increase in the neutrino temperature and therefore results in a modification on the value of N_{eff} at the time of BBN [13]. Since the contribution from dark radiation is only relevant when the ALPs are close to thermal equilibrium, we can parametrize the deviation from ΛCDM as

$$\Delta N_{\mathrm{eff}}^{\mathrm{BBN}} \approx \frac{\rho_a}{\rho_\gamma} \approx \frac{\rho_a^{eq} n_a}{\rho_\gamma n_a^{eq}} \tag{4.1}$$

where ρ_γ is the energy density in photons at BBN. Though N_{eff} is not directly measured at BBN, it can inferred from the measured value at recombination by Planck [43], to be [44] $N_{\mathrm{eff}}^{\mathrm{BBN}} = 2.86 \pm 0.15$, hence we set an upper bound on the ALP abundance at BBN by requiring $\Delta N_{\mathrm{eff}}^{\mathrm{BBN}} \lesssim 0.2$.

4.2 Cosmic Microwave Background

After the end of BBN, any particle that injects energy in the primordial plasma will modify, to some extent, the observations of the CMB. The impact of energy injected before recombination would work to heat up the plasma and hence cause changes to the observed anisotropies in the CMB power spectrum. However, since the major source of energy injected is via ALP decays to neutrinos, the energy injected into the photon bath is negligible, and thus we do not expect constraints arising from CMB anisotropies. Late time decays of ALPs could also cause spectral distortions in the black body spectrum of the CMB if the decays heat up the photon bath significantly [39]. Fortunately, as before, the decay rate from ALPs to photons is negligible and we assume that secondary energy injected into the photon spectrum from the decays of ALPs can be safely ignored.

The most significant impact of the decays of ALPs for recombination is the modification of the neutrino temperature. Since neutrino decoupling, the photon and neutrino temperatures evolved independently which, even in ΛCDM, causes a value of the effective neutrino degrees of freedom as $N_{\text{eff}} = 3.044 \pm 0.384$ [43]. ALP decays before the formation of the CMB increase the neutrino temperature, as in eq.(3.11). This increase of the temperature of the neutrino bath with respect to that of the photon bath, causes the value of N_{eff} to increase from the expectations of ΛCDM, as

$$N_{\text{eff}}^{\text{CMB}} = N_{\text{eff}}^{\text{BBN}} \left(\frac{11}{4} \right)^{\frac{4}{3}} \left(\frac{T_\nu}{T_\gamma} \right)^4 \tag{4.2}$$

which strongly constraints the decay rate of ALPs.

Lastly, from observations of the CMB, the abundance of non-baryonic matter (dark matter) was observed to be around $\Omega_{\text{DM}} \sim 0.12$. ALPs that become non-relativistic before recombination, and they have lifetimes larger than $\tau_a > 10^{13}$ s, would survive long enough to contribute their abundance to that of dark matter. Therefore this also sets a strong constraint on the total abundance of ALPs at the time of recombination, which is partially complementary to the constraint on N_{eff}.

4.3 SN1897A

The core of supernovae (SN) are very hot and dense systems, with temperatures of the order of $T \sim 30$ MeV. Most of the particles created in such energetic medium are trapped and contribute to the energy transfer inside the SN core. Weakly coupled particles, however, can free-stream and escape the core, contributing to the cooling of the SN. The primary source of cooling for SNs are neutrinos, which can escape as long as they have energies $E_\nu \lesssim 30$ MeV. This neutrino burst was observed for SN1987A by various water Cherenkov detectors, including Kamiokande-II [45, 46]. Besides neutrinos, the HNLs and ALPs in our model could also escape the SN core as they interact very weakly with the SN inner medium, and contribute to SN cooling [47–52]. This additional source of cooling is very constrained by measurements of the luminosity of SN187A. Secondary decays of HNLs and ALPs into neutrinos produce a high-energetic additional flux of active neutrinos that could have been detected alongside the normal neutrino burst [50, 51]. The combination of SN cooling and the additional neutrino flux can impose strong constraints on our model for high couplings.

For both HNLs and ALPs, the constraint on the secondary neutrino flux is much stronger than the constraint from SN cooling [51, 52], and hence we only include the former in our study. Typical constraints on the secondary neutrino flux from HNL decays assume decay rates for HNLs in the absence of additional channels, so the $N \to \pi\nu$ and $N \to 3\nu$ decays dominates [49]. In our model the primary decay channel for HNLs is to ALPs, which consecutively decay to a pair of neutrinos. Hence, neglecting resonant effects, the secondary neutrino flux from HNLs can be approximated to that arising from the 3-body decay of the HNLs to neutrinos. Even though the 2-body decay branching ratio is around 7 times larger than the 3-body decays for HNL masses in the 100 MeV range,

Cherenkov detectors are more sensitive to the 3-body decays, since the interaction cross section of antineutrinos, only produced in 3-body decays, is around 100 times larger than that of neutrinos [45]. Therefore, SN limits on traditional HNL decays can be directly applied to our scenario. We thus use the limits on HNL masses and mixing from Fig. 2 of [52] to constrain the large mixing angle regions in our model.

In addition to HNLs, ALPs can also be produced in the core of SN. The expected secondary neutrino flux from decaying ALPs with masses below the keV scale is smaller than that from HNL decays that can escape the SN core. However, heavy HNLs cannot escape and thus SN constraints from the production of ALPs are stronger for $m_N \gtrsim 400$ MeV. From Fig. 5 of [52], we can see that the coupling between the ALP and the electron-neutrino g_{ae} must be $g_{ae} \lesssim 10^{-7}$ for keV-scale ALPs. In our model, g_{ae} is given by Eq. (2.26), which imposes only weak limits for heavy HNLs and large HNL-ALP couplings, beyond the ranges considered in our study.

Lastly, there could be additional constraints from secondary decays of HNLs and/or ALPs to photons [53]. However, these are negligible as the photonic branching ratios of both particles are very small for the masses considered.

4.4 Other astrophysical constraints

In addition to the astrophysical constraints from SN cooling and its secondary fluxes, there is a plethora of possible astrophysical probes of ALPs. The production of ALP in the core of white dwarfs or RGB stars can lead to strong cooling, and even provide an explanation for the observed cooling hints [54, 55]. In fact, it has been shown that an ALP with a coupling to electrons of the order $g_{ae} \sim 10^{-13}$ provides a good fit to stellar cooling data [55]. However, in our model the ALP-electron coupling is very small, so much that the value $g_{ae} \sim 10^{-13}$ can only be reached for mixing $|U_{eN}|^2 \sim 10^{-1}$ and HNL masses $m_N \sim 1$ TeV. Since this parameter region is beyond our scope, and anyways disfavoured by various cosmological constraints, as we will see later, we neglect the constraints from stellar cooling in our study.

Long-lived ALPs that survive after recombination may still be observable today through their decay products. The photons injected by ALP decays are the most detectable candidates, as they can be probed in observations of the extra-galactic background light (EBL) or via X-rays [36]. For ALP masses below the keV scale, the constraints on the ALP-photon coupling from X-ray and EBL surveys require that $g_{a\gamma} \lesssim 10^{-15}$ GeV^{-1} [36, 39]. In our model, however, the ALP-photon coupling is derived at two-loop order, and therefore extremely small. As above, only for very large mixing $U_{eN}^2 \sim 10^{-3}$ and large HNL masses $m_N \sim 1$ TeV, has this constraint any effect. Consequently, we also ignore any astrophysical constraints from late-time photonic decays of ALPs.

4.5 Impact on direct HNL searches

Future HNL searches, especially those based on long-lived signatures, will probe small active-sterile mixing strengths approaching the seesaw expectation. Prominent examples of proposed and planned searches are PIONEER [56], NA62 [57, 58], DUNE [59], SHiP [60], FCC-ee [61]. A dedicated analysis is needed to present a study of the sensitivity in

our scenario depending on the specific search strategy. Such a detailed analysis is beyond the scope of this paper and will be considered as future work. In this section, we will assess how the sensitivity is modified in presence of new HNL-ALP coupling in the context of DUNE. We qualitatively describe the approach to calculate the expected number of signal events in the DUNE near detector (ND) based on the analysis [62]. The ND is located at a distance of $L = 574$ m from the HNL production point, with a transverse cross-section of $A = 12$ m^2 and a depth of $\Delta L = 5$ m along the beam axis. Following [62], we write the expected number of signal events as

$$N_{\text{sig}} = N_P \times \text{Br}(\text{P} \to \text{N}) \times \text{Br}(\text{N} \to \text{charged}) \times \epsilon_{\text{geo}}, \tag{4.3}$$

where N_P is the relevant production fraction of positively-charged and neutral pseudoscalar mesons multiplied by the total number of protons on target $N_{\text{POT}} = 6.6 \times 10^{21}$ for a 120 GeV proton beam at DUNE, $\text{Br}(\text{P} \to \text{N})$ is the branching fractions of HNL production from the meson P, $\text{Br}(\text{N} \to \text{charged})$ is the branching fraction of produced HNL decaying into charged lepton pairs and ϵ_{geo} corresponds to the geometrical efficiency,

$$\epsilon_{\text{geo}} = e^{-\frac{m_N \Gamma_N}{p_{N_z}} L} \left(1 - e^{-\frac{m_N \Gamma_N}{p_{N_z}} \Delta L} \right). \tag{4.4}$$

Here, p_{N_z} is the momentum of the HNL along the beam axis in the lab frame, where we have considered $p_{N_z} = 7.5$ GeV, following the simulation of meson production from a pp collision at $\sqrt{s} = 15$ GeV [62]. As we have not explicitly simulated any events and analysed with respect to detector level cuts, for simplicity we will consider, in our analysis, that all produced HNL events will be accepted at detector level.

In presence of the HNL-ALP coupling as well as the new HNL decay channel $N \to a\nu$ in our scenario, the corresponding total decay width will also be affected. Correspondingly, the partial decay width of HNLs decaying into visible final states as well as the geometrical efficiency factor will change. In contrast, the production rate N_P as well as the branching ratio of HNL production from mesons is unaffected. We thus consider the relative change in the number of events,

$$\frac{N'_{\text{sig}}}{N_{\text{sig}}} = \frac{\text{Br}'(\text{N} \to \text{charged})}{\text{Br}(\text{N} \to \text{charged})} \frac{\epsilon'_{\text{geo}}}{\epsilon_{\text{geo}}} \tag{4.5}$$

where the unprimed and primed quantities correspond to $\Gamma_N \equiv \Gamma^{N \to \text{SM}}$ and $\Gamma'_N \equiv \Gamma^{N \to \text{SM}} + \Gamma^{N \to a\nu}$, respectively, as discussed in Sec. 2.2. From Fig. 1, we can notice that for $(m_a, f_a) = (1\,\text{keV}, 1\,\text{TeV})$, the total decay width of the HNL is dominated by $N \to a\nu$ throughout the considered mass range, while for $(1\,\text{keV}, 10^{2.5}\,\text{TeV})$, up to $m_N \sim m_\pi$, $N \to a\nu$ dominates the scenario and beyond this point, it drops significantly. Furthermore, as the decay widths for $N \to a\nu$ and $N \to \text{SM}$ have the same U_{eN} dependence, the branching fractions are independent of U_{eN}.

Likewise, the ratio of the geometric efficiencies can be approximated by

$$\frac{\epsilon'_{\text{geo}}}{\epsilon_{\text{geo}}} = \exp\left[-\frac{m_N}{p_{N_z}} \Gamma(N \to a\nu) L \right] \frac{\Gamma'_N}{\Gamma_N}, \tag{4.6}$$

for a shallow detector depth ΔL, i.e., for $(m_N/p_{N_z})\Gamma'_N \Delta L \ll 1$. The ratio of decay rates in this expression is equal to $\Gamma'_N/\Gamma_N = \mathrm{Br}(N \to \mathrm{charged})/\mathrm{Br}'(\mathrm{N} \to \mathrm{charged})$, thus cancelling the corresponding ratio in Eq. (4.5) in this limit. We thus have

$$\frac{N'_{\mathrm{sig}}}{N_{\mathrm{sig}}} = \exp\left[-\frac{m_N}{p_{N_z}}\Gamma(N \to a\nu)L\right], \tag{4.7}$$

which approaches unity for long decay lengths, $(m_N/p_{N_z})\Gamma(N \to a\nu)L \ll 1$. Thus, for small $|U_{eN}|^2$ and m_N where $\Gamma(N \to a\nu) \ll p_{N_z}/(m_N L)$, we expect that DUNE will have the same sensitivity towards the active-sterile mixing strength $|U_{eN}|^2$ in our HNL-ALP scenario as in the standard HNL case. For shorter decay lengths, the sensitivity will be reduced.

As another example for a direct search experiment we consider the existing NA62 experiment which uses a different search strategy as compared to DUNE. The NA62 experiment [57] used a secondary 75 GeV hadron beam containing a fraction of kaons, and has been able to probe the decays $K^+ \to \ell^+ N$. For small active-sterile mixing the decay length of HNL is much larger than the 75 m detector size and the process is characterised by a single detected track, that of the charged lepton – a positive signal is a peak in its missing mass distribution. As this experiment is currently insensitive to the decay of the HNLs, the presence of the $N \to a\nu$ decay channel will not affect the search as long as the decay length remains large.

5 Results and discussion

The aim of this work is to find valid scenarios where the traditional BBN bound on HNLs [42] is relaxed due to the primary decays to ALPs. For this purpose we have performed some small scale parameter scans around the benchmark scenarios in Table 1 to illustrate this effect[3]. Figure 5 shows the results of these parameter scans, varying the values of $m_N = [10^{-3}, 10^2]$ GeV and $|U_{eN}|^2 = [10^{-13}, 10^{-6}]$. The top row corresponds to scans around scenarios 1 and 2, with only m_a and f_a fixed, and, where the blue diamond markers are the fixed values of m_N and $|U_{eN}|^2$ from Table 1. The bottom row shows scans of scenarios 3 and 4, which have a lighter ALP mass of $m_a = 10$ eV.

In all the panels of Fig. 5, the three different regimes of ALP decay lifetime (as discussed earlier) are shown. ALPs decaying before the end of BBN, i.e., $\tau_a < 10^4$ s, to the right of the $\tau_a = 10^4$ s line, are not considered in this study. As we will argue below, points in this region are excluded anyway due to the fast ALP decays, so in this way we are justified in neglecting scenarios with short-lived ALPs. As expected, since the lifetime of the ALP goes like $\sim f_a^2/m_a$, for the larger values of f_a in the right-hand panels and lower m_a values on the bottom panels, the excluded region for short ALP lifetimes moves to larger HNL masses and larger mixing. Additionally, the ALP lifetimes around the formation of the CMB, $\tau_a = 10^{13}$ s, and the age of the Universe, $\tau_a = 10^{17}$ s are shown.

---

[3]We performed a grid scan on two parameters of the model, m_N and $|U_{eN}|^2$. This simplification is enough for our purposes as we only intend to highlight the crucial features of the model, but do not attempt to map the available parameter space nor perform any statistical interpretation of the results. For more details on the rigorous treatment of inference and statistics in physics see [63].
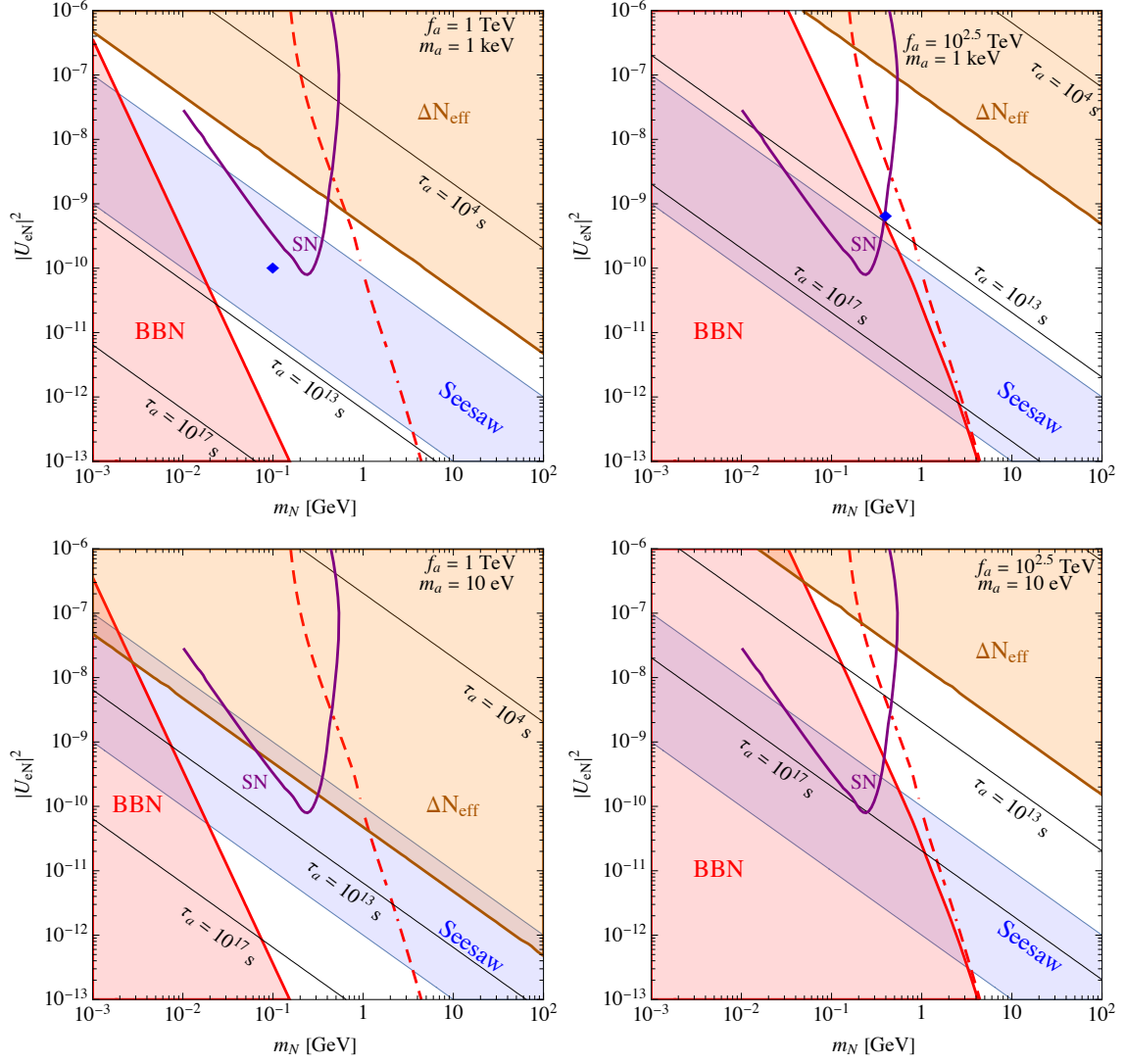
Figure 5. Allowed parameter regions in the m_N vs $|U_{eN}|^2$ plane for the four benchmark scenarios in Table 1: Upper left panel : $f_a = 1$ TeV, $m_a = 1$ keV, Upper right panel : $f_a = 10^{2.5}$ TeV, $m_a = 1$ keV, Lower left panel : $f_a = 1$ TeV, $m_a = 10$ eV, Lower right panel : $f_a = 10^{2.5}$ TeV, $m_a = 10$ eV. The red region shows the space disallowed by HNL decay time after the start of BBN, while the region left to red dashed contour is disfavored if HNL decays only via SM decay channels, in absence of ALP. The most stringent bound from cosmology, $N_{\text{eff}} < 3.10322 \, (\Lambda\text{CDM}) + 0.0384 \, (0.1\sigma_N)$ gives the brown forbidden region of active neutrinos produced from ALP decays. The region above the purple contour is excluded due to astrophysical constraints from supernova SN1987A. The seesaw regime for active neutrinos 1 meV $\lesssim m_\nu \lesssim$ 100 meV is shown in blue. The different black lines label the ALP decay time at 10^4 s (end of BBN), 10^{13} s (CMB) and 10^{17} s (today). Benchmark values from Tab.1 for scenario 1 and 2 with fixed m_N and $|U_{eN}|^2$ are denoted in top panels by blue diamonds.

The dashed red line corresponds to the HNL decay lifetime $\tau_N = 0.023$ s where only SM decay channels are present, i.e. in the absence of the ALP. Conversely, the solid red

line denotes the same HNL lifetime limit, but in the presence of the additional decay channel $N \to a\nu$. Since HNL decays after the start of BBN would modify the abundance of primordial elements, scenarios with longer lived HNLs are also not considered, and hence shaded in red in Fig. 5. Consequently, whenever the HNL to ALP decays dominate, the BBN limit is relaxed as compared to the standard scenario. This effect is more evident on the left-hand side panels, with $f_a = 1$ TeV, where the BBN limit is lowered by about two orders of magnitude with respect to vanilla HNL models. For larger f_a values, on the right-hand panels, the HNL-ALP coupling, which goes like $\sim 1/f_a$, is weaker and thus the exclusion due to the HNL lifetime is stronger as the impact of the addition of the ALP to the model is less significant.

In this article, for simplicity, we have only considered a single HNL, which is not enough to generate non-zero masses for all active neutrinos. Nevertheless, it is useful to show the expected mass scale of active neutrino mass generation, under the seesaw approximation. We thus show in Fig. 5 the blue shaded region for the seesaw mass 1 meV $\lesssim m_\nu \lesssim 100$ meV.

The strongest cosmological constraint, shown as the shaded brown region in the panels, arises from the increase on the neutrino temperature due to ALP decays, which shows as a modification of the N_{eff} at the time of recombination. N_{eff} constrains the larger HNL masses and mixing, corresponding to shorter ALP lifetimes. Consequently, ALPs decaying before the onset of BBN, or shortly after, would cause a sufficient increase of the neutrino temperature and be excluded by the Planck measurement of the N_{eff} value. Smaller HNL-ALP couplings cause longer ALP lifetimes, and thus the right-handed panels with larger f_a have weaker N_{eff} constraints. However, for the bottom panels with lower m_a, even though the lifetime is also longer and one would expect the limit to be weaken, the opposite effect occurs and the N_{eff} limit is significantly stronger. This happens because lighter ALPs are ultra-relativistic for a longer period between BBN and recombination, and thus have a stronger effect on the expansion rate, and thus on the neutrino temperature and value of N_{eff}. Other cosmological constraints such as, energy injection before BBN or the relic abundance of ALPs are subleading and thus not shown. The region above the purple contour is, in principle, excluded due to the astrophysical constraints from supernova SN1987A, arising from the modified neutrino flux due to the production of HNLs in the core of the supernova. Nevertheless, the uncertainties in the calculation of the SN neutrino flux are high and depend on the choice of SN core model [64], hence we show in purple a conservative expectation of the limit, but refrain from excluding models only on the basis of this SN constraint. Supernova constraints due to ALP production, which is largely independent of m_a in the ranges of interest, only apply for large values of $|U_{eN}|^2$ and m_N, which however resides well outside of our considered region.

The combination of all the overlaid constraints still leaves a significant region of the parameter space allowed, which becomes narrower for large values of $|U_{eN}|^2$ and wider for smaller values. The most interesting section of this allowed region corresponds to the one on the left of the BBN limit in vanilla HNL models (dashed red), which is the parameter space gained for lower HNL masses with the introduction of the additional decay channel $N \to a\nu$. The panels on the left, for $f_a = 1$ TeV, show a significant increase on the

viability of HNL masses, all the way down to $m_N \sim$ MeV, at the expense of stronger constraints on the mixing $|U_{eN}|^2$ due to the stronger HNL-ALP interactions. The newly open region is much narrower in the panels on the right, with $f_a = 10^{2.5}$ TeV, as the HNL-ALP interactions are much weaker, and only slightly relevant for high $|U_{eN}|^2$ values. On the other hand, stronger HNL-ALP interactions, for $f_a < 1$ TeV, would not provide any noticeable improvement, as the ALPs would then be produced in equilibrium and the cosmological constraints would be much stronger. In conclusion, from Fig. 5 there is a reasonable expectation for HNLs in our model to have masses at around the MeV scale without affecting the cosmological history of the Universe.

In Fig. 6 we present this newly available parameter region which may be the target of future dedicated searches for HNLs. In the left panel, we show the corresponding parameter space for scenario 1 ($f_a = 1$ TeV, $m_a = 1$ keV) as described in previous section, while the right panel corresponds to the scenario 2 ($f_a = 10^{2.5}$ TeV, $m_a = 1$ keV). The gray shaded regions in both panels are disfavored from various cosmological and astrophysical constraints discussed in Sec. 4, and shown coloured in Figure 5. The gray dashed curve denotes the BBN bound from the HNL only decaying to SM decay channels i.e., in absence of the ALP. The corresponding seesaw regime is shown in blue considering 1 meV $\lesssim m_\nu \lesssim$ 100 meV. The red dashed contour corresponds to the future sensitivity of DUNE HNL searches in standard HNL models (without ALPs), while the solid red contours in both panels denote the resultant sensitivity contours for observation of 6 events in presence of the new $N \to a\nu$ decay channel in respective benchmark scenarios with two different f_a values. Additionally, as described in Tab. 1, in blue diamonds two benchmark scenarios with fixed HNL mass and mixing $m_N = 10^{-1}$ GeV, $|U_{eN}|^2 = 10^{-10}$ and $m_N = 10^{-0.4}$ GeV, $|U_{eN}|^2 = 10^{-9.2}$, have been shown. The brown dashed contour denotes the present exclusion contour from NA62 experiment. Furthermore, considering the discussion of subsection 4.5, we have also highlighted in brown the region where the approximation holds (with $L_{\text{NA62}} = 75$ m and $p_{N_z} \sim 30$ GeV as the K^+ beams have energy ~ 75 GeV [57]), the present sensitivity contour remains unaffected by the new axion decay channel of HNL in this region. From Figure 6 it is evident that the available regions constrained by several astrophysical and cosmological constraints can be well probed in the future by DUNE and NA62 in presence of this new decay channel of HNLs.

6 Conclusions and outlook

In this work we have presented a simplified model of new physics including a single HNL, which mixes with a light active neutrino in a seesaw scenario, and an axion-like particle, whose only tree-level interaction is with the HNL. This model is motivated to explore the potential impact on the decay rate of the HNL allowing to evade constraints from BBN for HNL masses around the MeV scale. This would open up parameter space probed by HNL direct searches that is otherwise disfavoured by cosmological considerations. However, the ALPs produced by the scattering and decay of HNLs can have a significant impact on the evolution of the Universe, as they affect its expansion rate and their own decays increase the temperature of the neutrino bath. Further constraints on the model arise from the
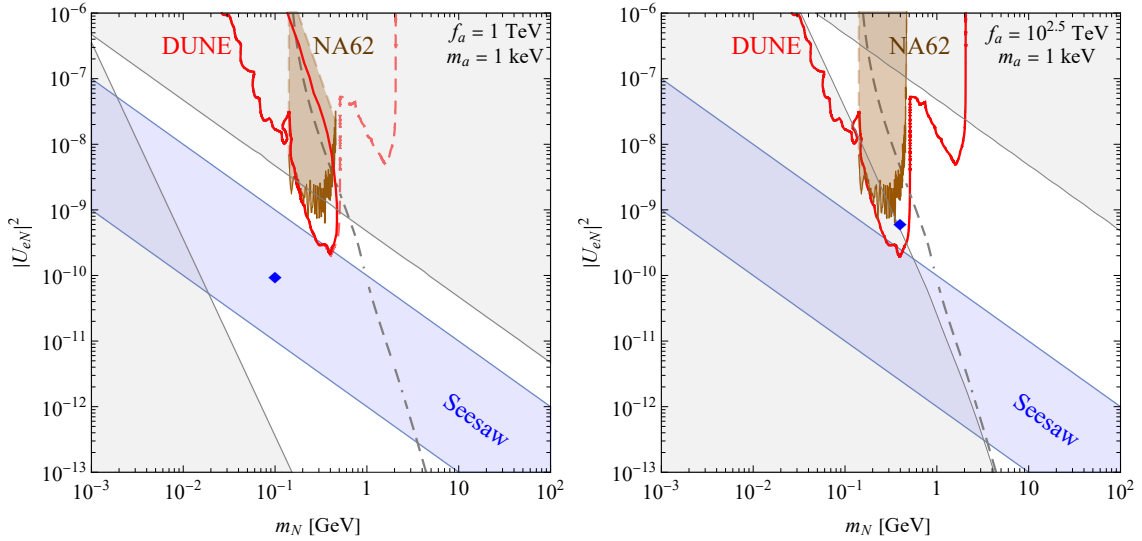
Figure 6. The sensitivity contours of future DUNE and current NA62 searches for observation of 6 events in newly available parameter space constrained by several astrophysical and cosmological constraints (gray shaded region) for two different benchmark scenarios i.e., left panel ($f_a = 1$ TeV, $m_a = 1$ keV) and right panel ($f_a = 10^{2.5}$ TeV, $m_a = 1$ keV). The region left to gray dashed contour is disfavored if HNL decays only via SM decay channels, in absence of ALP. The seesaw regime for active neutrinos 1 meV $\lesssim m_\nu \lesssim$ 100 meV is shown in blue. Benchmark values from Tab.1 for scenario 1 and 2 with fixed m_N and $|U_{eN}|^2$ are denoted in two panels by blue diamonds. The red solid (dashed) contours denote the DUNE sensitivity contours with (without) HNL to ALP decay channel. The brown contour corresponds to NA62 present sensitivity while the brown shaded region denotes the unaffected parameter space, in presence of $N \rightarrow a\nu$ channel, using the approximation discussed in subsection 4.5.

production of ALPs in the core of stars or supernovae, which is strongly constrained from the observation of the photon and neutrino fluxes from SN1987A.

We have thus found that, in spite of the strong constraints, there is viable parameter space in the region of interest where the ALPs are not produced abundantly enough to modify the cosmology of the Universe significantly. They nevertheless open up a new and dominant decay channel for the HNLs so that they decay non-hadronically and are not constrained by BBN. The relaxation of the BBN limit compared to the standard HNL model is more significant for stronger HNL-ALP interactions ($f_a = 1$ TeV), where HNL masses around $m_N \sim$ MeV are allowed, with a relatively large active-sterile mixing.

This region of parameter space with HNL masses 1 MeV $< m_N <$ 1 GeV and couplings $10^{-10} < |U_{eN}|^2 < 10^{-7}$, which is allowed in our model in contrast to the vanilla HNL model, is a prime target for direct searches for HNLs at colliders, fixed target and beam dump experiments. While a detailed analysis is beyond the scope of this work, we discuss the constraints from the existing NA62 search and the expected sensitivity of a future search at the DUNE near detector. We find that the additional decay to ALPs significantly alters the probed parameter space but as long the HNL remains sufficiently long-lived, i.e., for $m_N \approx 100$ MeV to 1 GeV, both experiments still probe small active-sterile mixing strengths

$|U_{eN}|^2 \approx 10^{-9}$.

Our simplified model motivates the search for lighter HNLs within a region otherwise disfavoured by BBN constraints. It also shows that, once allowing the HNL to couple to a light dark sector, the phenomenology, specifically as a long-lived particle can change significantly, and searches should consider non-standard decay lengths and exotic decay modes. This is in correlation with cosmological observations and future improvements in this sector are expected to tighten the presence of a light sector.

Acknowledgments

A   Calculation of decay and scattering rates

In this appendix, we will give analytical expressions for the scattering cross-sections involving active neutrinos, HNL and ALP in all possible way. Due to the couplings presented in Eq.(2.9) one can also consider the axion-HNL scattering in early universe. The process happens via t-channel scattering. The matrix element responsible for the process $a(p_1) + a(p_2) \to N(p_3, s) + N(p_4, r)$ can be written as

$$\mathcal{M}_t = \frac{4m_N^2}{f_a^2} \left(\bar{u}_3^s \frac{\slashed{q} - m_N}{q^2 - m_N^2} u_4^r \right) \tag{A.1}$$

where momentum exchange is $q^2 \equiv (p_1 - p_3)^2 = t$. Now finding $|\mathcal{M}_t|^2$ and performing the sum over final spin states s, r of HNLs one gets

$$\sum_{r,s} |\mathcal{M}_t|^2 = \frac{64m_N^4}{f_a^4(t - m_N^2)^2} \Big[2(p_3.q)(p_4.q) - (p_3.p_4)(q.q - m_N^2) + 2m_N^2(p_3.q) + 2m_N^2(p_4.q) + m_N^2(q.q + m_N^2) \Big] \tag{A.2}$$

Now, putting the definitions for kinematic variables and phase space factor as well as integrating over the angular variables, we get the total cross-section as

$$\sigma_{aaNN} = \frac{4m_N^4 \sqrt{s - 4m_a^2}}{\pi f_a^4 s^{3/2}} \Bigg[-1 - \frac{m_a^4 - 4m_a^2 m_N^2}{m_a^4 - 4m_a^2 m_N^2 + m_N^2 s} + \frac{2(s - 2m_a^2)\coth^{-1}\left(\frac{s - 2m_a^2}{\sqrt{s - 4m_a^2}\sqrt{s - 4m_N^2}} \right)}{\sqrt{s - 4m_a^2}\sqrt{s - 4m_N^2}} \Bigg]. \tag{A.3}$$

– 25 –

Similarly, for the inverse scattering $N(p_1, s) + N(p_2, r) \to a(p_3) + a(p_4)$ we have

$$\sigma_{NNaa} = \frac{4m_N^4}{\pi f_a^4 s^{3/2}} \left[-\frac{\sqrt{s - 4m_N^2}(2m_a^4 - 8m_a^2 m_N^2 + m_N^2 s)}{m_a^4 - 4m_a^2 m_N^2 + m_N^2 s} \right.$$
$$\left. + \frac{2(s - 2m_a^2)\coth^{-1}\left(\frac{s - 2m_a^2}{\sqrt{s - 4m_a^2}\sqrt{s - 4m_N^2}}\right)}{\sqrt{s - 4m_a^2}} \right], \tag{A.4}$$

where $s \equiv (p_1 + p_2)^2 = (p_3 + p_4)^2$. Likewise, for $aa \to \nu\nu$ scattering with t-channel HNL mediation,

$$\sigma_{aa\nu\nu} = \frac{4m_N^4 \sqrt{s - 4m_a^2} U_{eN}^4}{\pi f_a^4 s^{3/2}}$$
$$\times \left[-\frac{2(m_a^4 + m_N^4 + m_\nu^4 - 2m_a^2 m_N^2 - 2m_a^2 m_\nu^2 - 2m_N^2 m_\nu^2) + m_N^2 s}{m_a^4 + m_N^4 + m_\nu^4 - 2m_a^2 m_N^2 - 2m_a^2 m_\nu^2 - 2m_N^2 m_\nu^2 + m_N^2 s} \right.$$
$$\left. + \frac{2(2(m_a^2 - m_N^2 + m_\nu^2) - s)\coth^{-1}\left(\frac{2(m_a^2 - m_N^2 + m_\nu^2) - s}{\sqrt{s - 4m_a^2}\sqrt{s - 4m_\nu^2}}\right)}{\sqrt{s - 4m_a^2}\sqrt{s - 4m_\nu^2}} \right]. \tag{A.5}$$

In the limit, $m_\nu \to 0$, we will get simplified expression for $aa \to \nu\nu$ scattering as

$$\sigma_{aa\nu\nu} = \frac{4m_N^4 \sqrt{s - 4m_a^2} U_{eN}^4}{\pi f_a^4 s^{3/2}} \left[-\frac{2(m_a^4 + m_N^4 - 2m_a^2 m_N^2) + m_N^2 s}{m_a^4 + m_N^4 - 2m_a^2 m_N^2 + m_N^2 s} \right.$$
$$\left. + \frac{2(2(m_a^2 - m_N^2) - s)\coth^{-1}\left(\frac{2(m_a^2 - m_N^2) - s}{\sqrt{s - 4m_a^2}\sqrt{s}}\right)}{\sqrt{s - 4m_a^2}\sqrt{s}} \right]. \tag{A.6}$$

The cross-section for $aa \to \nu N$ scattering (in the limit $m_\nu \to 0$) with t-channel HNL mediation,

$$\sigma_{aa\nu N} = \frac{2m_N^4 \sqrt{s - 4m_a^2} U_{eN}^2}{\pi f_a^4 s^{3/2}} \left[-\frac{2(2m_a^4 - 7m_a^2 m_N^2 + 5m_N^4 + m_N^2 s)}{m_a^4 - 2m_a^2 m_N^2 + m_N^4 + m_N^2 s} \right.$$
$$\left. + \frac{4(2m_a^2 - 4m_N^2 - s)\coth^{-1}\left(\frac{2(m_a^2 - m_N^2) - s}{\sqrt{s - 4m_a^2}\sqrt{s}}\right)}{\sqrt{s - 4m_a^2}\sqrt{s}} \right]. \tag{A.7}$$

The cross-section for $aa \to NN$ scattering (in the limit $m_\nu \to 0$) with t-channel ν mediation,

$$\sigma_{aaNN} = \frac{4m_N^4 \sqrt{s - 4m_a^2} U_{eN}^4}{\pi f_a^4 s^{3/2}} \left[-\frac{2m_a^4 - 4m_a^2 m_N^2 + 4m_N^4 - m_N^2 s}{m_a^4 - 2m_a^2 m_N^2 + m_N^4} \right.$$
$$\left. + \frac{2(2(m_a^2 + m_N^2) - s)\coth^{-1}\left(\frac{2(m_a^2 + m_N^2) - s}{\sqrt{s - 4m_a^2}\sqrt{s - 4m_N^2}}\right)}{\sqrt{s - 4m_a^2}\sqrt{s - 4m_N^2}} \right]. \tag{A.8}$$

The cross-section for $aa \to \nu\nu$ scattering (in the limit of $m_\nu \to 0$) with t-channel ν mediation,

$$\sigma_{aa\nu\nu} = \frac{4m_N^4 \sqrt{s - 4m_a^2} U_{eN}^8}{\pi f_a^4 s^{3/2}} \left[-2 + \frac{2(s - 2m_a^2)\coth^{-1}\left(\frac{s - 2m_a^2}{\sqrt{s - 4m_a^2}\sqrt{s}}\right)}{\sqrt{s - 4m_a^2}\sqrt{s}} \right]. \tag{A.9}$$

The cross-section for $aa \to \nu N$ scattering (in the limit $m_\nu \to 0$) with t-channel ν mediation,

$$\sigma_{aa\nu N} = \frac{4m_N^4 \sqrt{s - 4m_a^2} U_{eN}^6}{\pi f_a^4 s^{3/2}} \left[-2 + \frac{m_N^2}{m_a^2} + \frac{2(s - 2m_a^2)\coth^{-1}\left(\frac{s - 2m_a^2}{\sqrt{s - 4m_a^2}\sqrt{s}}\right)}{\sqrt{s - 4m_a^2}\sqrt{s}} \right]. \tag{A.10}$$

The cross-section for $\nu\nu \to NN$ scattering (in the limit $m_\nu \to 0$) with t-channel axion mediation,

$$\sigma_{\nu\nu NN} = \frac{m_N^4 U_{eN}^4}{\pi f_a^4 s} \left[\frac{2m_a^4 + 2m_N^4 + m_N^2 s + 2m_a^2(s - 2m_N^2)}{m_a^4 + m_N^4 + m_a^2(s - 2m_N^2)} \right.$$
$$\left. + \frac{2(s + 2m_a^2 - 2m_N^2)\coth^{-1}\left(\frac{-2m_a^2 + 2m_N^2 - s}{\sqrt{s - 4m_N^2}\sqrt{s}}\right)}{\sqrt{s - 4m_N^2}\sqrt{s}} \right]. \tag{A.11}$$

The cross-section for $a\nu \to aN$ (in the limit $m_\nu \to 0$) with s and t-channel HNL mediation,

$$\sigma_{a\nu aN} = \frac{m_N^4 U_{eN}^2}{2\pi f_a^4 (m_N^2 - s)^2 s}$$
$$\times \left[\frac{1}{m_a^4 - 4m_a^2 m_N^2 + m_N^2 s} \right.$$
$$\left\{ 2m_a^8 + m_N^2(8m_N^6 - 20m_N^4 s + 15m_N^2 s^2 + (5 - 2m_N^2)s^3 + 2s^4) \right.$$
$$+ 2m_a^2(3m_N^6 + 6m_N^4(s - 1)s - 6m_N^2 s^2(3 + s)) + 2m_a^6(2m_N^2(s - 3)$$
$$\left. - s(3 + 2s)) + m_a^4(2m_N^4(7 - 8s) + s^2(7 + 2s) + m_N^2 s(29 + 14s)) \right\}$$
$$- 4\sqrt{\frac{s - m_N^2}{s - 4m_a^2}} \left\{ 2m_a^4 + m_N^4(3 - 2s) - s^2 + 2m_N^2 s(s + 3) - m_a^2(3s \right.$$
$$\left. \left. + m_N^2(3 + 4s)) \right\} \coth^{-1}\left(\frac{s - 2m_a^2}{\sqrt{s - 4m_a^2}\sqrt{s - 4m_N^2}} \right) \right]. \tag{A.12}$$

References

[1] P. Minkowski, $\mu \to e\gamma$ *at a Rate of One Out of* 10^9 *Muon Decays?*, *Phys. Lett. B* **67** (1977) 421.

[2] R.N. Mohapatra and G. Senjanovic, *Neutrino Mass and Spontaneous Parity Nonconservation*, *Phys. Rev. Lett.* **44** (1980) 912.

[3] M. Gell-Mann, P. Ramond and R. Slansky, *Complex Spinors and Unified Theories*, *Conf. Proc. C* **790927** (1979) 315 [1306.4669].

[4] T. Yanagida, *Horizontal gauge symmetry and masses of neutrinos*, *Conf. Proc. C* **7902131** (1979) 95.

[5] J. Schechter and J.W.F. Valle, *Neutrino Masses in SU(2) × U(1) Theories*, *Phys. Rev. D* **22** (1980) 2227.

[6] M. Fukugita and T. Yanagida, *Baryogenesis Without Grand Unification*, *Phys. Lett. B* **174** (1986) 45.

[7] PARTICLE DATA GROUP collaboration, *Review of particle physics*, *Phys. Rev. D* **110** (2024) 030001.

[8] I. Esteban, M.C. Gonzalez-Garcia, M. Maltoni, T. Schwetz and A. Zhou, *The fate of hints: updated global analysis of three-flavor neutrino oscillations*, *JHEP* **09** (2020) 178 [2007.14792].

[9] P.D. Bolton, F.F. Deppisch and P.S. Bhupal Dev, *Neutrinoless double beta decay versus other probes of heavy sterile neutrinos*, *JHEP* **03** (2020) 170 [1912.03058].

[10] A.M. Abdullahi et al., *The present and future status of heavy neutral leptons*, *J. Phys. G* **50** (2023) 020501 [2203.08039].

[11] M. Chrzaszcz, M. Drewes, T.E. Gonzalo, J. Harz, S. Krishnamurthy and C. Weniger, *A frequentist analysis of three right-handed neutrinos with GAMBIT*, *Eur. Phys. J. C* **80** (2020) 569 [1908.02302].

[12] A. Boyarsky, M. Ovchynnikov, N. Sabti and V. Syvolap, *When feebly interacting massive particles decay into neutrinos: The Neff story*, *Phys. Rev. D* **104** (2021) 035006 [2103.09831].

[13] GAMBIT COSMOLOGY WORKGROUP collaboration, *CosmoBit: A GAMBIT module for computing cosmological observables and likelihoods*, *JCAP* **02** (2021) 022 [2009.03286].

[14] A. Atre, T. Han, S. Pascoli and B. Zhang, *The Search for Heavy Majorana Neutrinos*, *JHEP* **05** (2009) 030 [0901.3589].

[15] P. Coloma, E. Fernández-Martínez, M. González-López, J. Hernández-García and Z. Pavlovic, *GeV-scale neutrinos: interactions with mesons and DUNE sensitivity*, *Eur. Phys. J. C* **81** (2021) 78 [2007.03701].

[16] T. Hsyu, R.J. Cooke, J.X. Prochaska and M. Bolte, *The PHLEK Survey: A New Determination of the Primordial Helium Abundance*, *Astrophys. J.* **896** (2020) 77 [2005.12290].

[17] A. Davidson, *B − L as the fourth color within an* $SU(2)_L \times U(1)_R \times U(1)$ *model*, *Phys. Rev. D* **20** (1979) 776.

[18] R.E. Marshak and R.N. Mohapatra, *Quark - Lepton Symmetry and B-L as the U(1) Generator of the Electroweak Symmetry Group*, *Phys. Lett. B* **91** (1980) 222.

[19] R.N. Mohapatra and R.E. Marshak, *Local B-L Symmetry of Electroweak Interactions, Majorana Neutrinos and Neutron Oscillations*, *Phys. Rev. Lett.* **44** (1980) 1316.

[20] A. Davidson and K.C. Wali, *Universal Seesaw Mechanism?*, *Phys. Rev. Lett.* **59** (1987) 393.

[21] W. Buchmuller, C. Greub and P. Minkowski, *Neutrino masses, neutral vector bosons and the scale of B-L breaking*, *Phys. Lett. B* **267** (1991) 395.

[22] J.C. Pati and A. Salam, *Is Baryon Number Conserved?*, *Phys. Rev. Lett.* **31** (1973) 661.

[23] J.C. Pati and A. Salam, *Unified Lepton-Hadron Symmetry and a Gauge Theory of the Basic Interactions*, *Phys. Rev. D* **8** (1973) 1240.

[24] J.C. Pati and A. Salam, *Lepton Number as the Fourth Color*, *Phys. Rev. D* **10** (1974) 275.

[25] R.N. Mohapatra and J.C. Pati, *A Natural Left-Right Symmetry*, *Phys. Rev. D* **11** (1975) 2558.

[26] G. Senjanovic and R.N. Mohapatra, *Exact Left-Right Symmetry and Spontaneous Violation of Parity*, *Phys. Rev. D* **12** (1975) 1502.

[27] D.J.E. Marsh, *Axion Cosmology*, *Phys. Rept.* **643** (2016) 1 [1510.07633].

[28] F. Chadha-Day, J. Ellis and D.J.E. Marsh, *Axion dark matter: What is it and why now?*, *Sci. Adv.* **8** (2022) abj3618 [2105.01406].

[29] D.J.E. Marsh, *Axions for amateurs*, *Contemp. Phys.* **64** (2023) 1 [2308.16003].

[30] S. Gola, S. Mandal and N. Sinha, *ALP-portal majorana dark matter*, *Int. J. Mod. Phys. A* **37** (2022) 2250131 [2106.00547].

[31] G.B. Gelmini, S. Nussinov and T. Yanagida, *Does Nature Like Nambu-Goldstone Bosons?*, *Nucl. Phys. B* **219** (1983) 31.

[32] P. Gondolo and G. Gelmini, *Cosmic abundances of stable particles: Improved analysis*, *Nucl. Phys. B* **360** (1991) 145.

[33] M. Escudero, *Neutrino decoupling beyond the Standard Model: CMB constraints on the Dark Matter mass with a fast and precise $N_{\rm eff}$ evaluation*, *JCAP* **02** (2019) 007 [1812.05605].

[34] M. Hufnagel, K. Schmidt-Hoberg and S. Wild, *BBN constraints on MeV-scale dark sectors. Part II. Electromagnetic decays*, *JCAP* **11** (2018) 032 [1808.09324].

[35] M. Escudero Abenza, *Precision early universe thermodynamics made simple: $N_{\rm eff}$ and neutrino decoupling in the Standard Model and beyond*, *JCAP* **05** (2020) 048 [2001.04466].

[36] D. Cadamuro and J. Redondo, *Cosmological bounds on pseudo Nambu-Goldstone bosons*, *JCAP* **02** (2012) 032 [1110.2895].

[37] M. Drewes and B. Garbrecht, *Combining experimental and cosmological constraints on heavy neutrinos*, *Nucl. Phys. B* **921** (2017) 250 [1502.00477].

[38] P.F. Depta, M. Hufnagel and K. Schmidt-Hoberg, *Updated BBN constraints on electromagnetic decays of MeV-scale particles*, *JCAP* **04** (2021) 011 [2011.06519].

[39] C. Balázs et al., *Cosmological constraints on decaying axion-like particles: a global analysis*, *JCAP* **12** (2022) 027 [2205.13549].

[40] F. Iocco, G. Mangano, G. Miele, O. Pisanti and P.D. Serpico, *Primordial Nucleosynthesis: from precision cosmology to fundamental physics*, *Phys. Rept.* **472** (2009) 1 [0809.0631].

[41] A. Coc and E. Vangioni, *Primordial nucleosynthesis*, *Int. J. Mod. Phys. E* **26** (2017) 1741002 [1707.01004].

[42] A. Boyarsky, M. Ovchynnikov, O. Ruchayskiy and V. Syvolap, *Improved big bang nucleosynthesis constraints on heavy neutral leptons*, *Phys. Rev. D* **104** (2021) 023517 [2008.00749].

[43] Planck collaboration, *Planck 2018 results. VI. Cosmological parameters*, *Astron. Astrophys.* **641** (2020) A6 [1807.06209].

[44] B.D. Fields, K.A. Olive, T.-H. Yeh and C. Young, *Big-Bang Nucleosynthesis after Planck*, *JCAP* **03** (2020) 010 [1912.01132].

[45] Kamiokande-II collaboration, *Observation of a Neutrino Burst from the Supernova SN 1987a*, *Phys. Rev. Lett.* **58** (1987) 1490.

[46] Y. Totsuka et al., *Observation of a neutrino burst from the supernova SN1987a*, *Nucl. Phys. A* **478** (1988) 189.

[47] A.D. Dolgov, S.H. Hansen, G. Raffelt and D.V. Semikoz, *Cosmological and astrophysical bounds on a heavy sterile neutrino and the KARMEN anomaly*, *Nucl. Phys. B* **580** (2000) 331 [hep-ph/0002223].

[48] G.M. Fuller, A. Kusenko and K. Petraki, *Heavy sterile neutrinos and supernova explosions*, *Phys. Lett. B* **670** (2009) 281 [0806.4273].

[49] L. Mastrototaro, A. Mirizzi, P.D. Serpico and A. Esmaili, *Heavy sterile neutrino emission in core-collapse supernovae: Constraints and signatures*, *JCAP* **01** (2020) 010 [1910.10249].

[50] D.F.G. Fiorillo, G.G. Raffelt and E. Vitagliano, *Strong Supernova 1987A Constraints on Bosons Decaying to Neutrinos*, *Phys. Rev. Lett.* **131** (2023) 021001 [2209.11773].

[51] V. Syvolap, *Testing heavy neutral leptons produced in the supernovae explosions with future neutrino detectors*, 2301.07052.

[52] K. Akita, S.H. Im, M. Masud and S. Yun, *Limits on heavy neutral leptons, Z' bosons and majorons from high-energy supernova neutrinos*, *JHEP* **07** (2024) 057 [2312.13627].

[53] S. Hoof and L. Schulz, *Updated constraints on axion-like particles from temporal information in supernova SN1987A gamma-ray data*, *JCAP* **03** (2023) 054 [2212.09764].

[54] M. Giannotti, I. Irastorza, J. Redondo and A. Ringwald, *Cool WISPs for stellar cooling excesses*, *JCAP* **05** (2016) 057 [1512.08108].

[55] L. Di Luzio, M. Giannotti, E. Nardi and L. Visinelli, *The landscape of QCD axion models*, *Phys. Rept.* **870** (2020) 1 [2003.01100].

[56] PIONEER collaboration, *PIONEER: Studies of Rare Pion Decays*, 2203.01981.

[57] K. Dias, *Search for Heavy Neutral Lepton Production in NA62#*, *Moscow Univ. Phys. Bull.* **77** (2022) 220.

[58] M. Drewes, J. Hajer, J. Klaric and G. Lanfranchi, *NA62 sensitivity to heavy neutral leptons in the low scale seesaw model*, *JHEP* **07** (2018) 105 [1801.04207].

[59] P. Ballett, T. Boschi and S. Pascoli, *Heavy Neutral Leptons from low-scale seesaws at the DUNE Near Detector*, *JHEP* **03** (2020) 111 [1905.00284].

[60] SHiP collaboration, *Sensitivity of the SHiP experiment to Heavy Neutral Leptons*, *JHEP* **04** (2019) 077 [1811.00930].

[61] A. Blondel et al., *Searches for long-lived particles at the future FCC-ee*, *Front. in Phys.* **10** (2022) 967881 [2203.05502].

[62] P.D. Bolton, F.F. Deppisch, M. Rai and Z. Zhang, *Probing the Nature of Heavy Neutral Leptons in Direct Searches and Neutrinoless Double Beta Decay*, 2212.14690.

[63] S.S. AbdusSalam et al., *Simple and statistically sound recommendations for analysing physical theories*, *Rept. Prog. Phys.* **85** (2022) 052201 [2012.09874].

[64] P. Carenza, G. Lucente, L. Mastrototaro, A. Mirizzi and P.D. Serpico, *Comprehensive constraints on heavy sterile neutrinos from core-collapse supernovae*, *Phys. Rev. D* **109** (2024) 063010 [2311.00033].